Multisensor Fault Diagnosis Leveraging Reinforced Evidential Jensen-Alpha Divergence under Dempster-Shafer Theory

Zhe Liu[1,2,3,*], Juan Liao[4], Lili Wang[5], Yulong Huang[1], Kai Liu[1,6], Himanshu Dhumras[7] and Wulfran Fendzi Mbasso[8,9,10]

[1] College of Mathematics and Computer, Xinyu University, Xinyu, 338004, China

[2] Jadara Research Center, Jadara University, Irbid, 21110, Jordan

[3] School of Computer Sciences, Universiti Sains Malaysia, Penang, 11800, Malaysia

[4] School of Big Data Engineering, Kaili University, Kaili, 556000, China

[5] School of Artificial Intelligence, Dongguan City University, Dongguan, 523000, China

[6] School of Transportation Engineering, East China Jiaotong University, Nanchang, 330013, China

[7] School of Management, Shanghai University, Shanghai, 200444, China

[8] Department of Biosciences, Saveetha School of Engineering, Saveetha Institute of Medical and Technical Sciences, Chennai, 602105, India

[9] Technology and Applied Sciences Laboratory, University of Douala, Douala, P.O. Box 8689, Cameroon

[10] Applied Science Research Center, Applied Science Private University, Amman, 11937, Jordan

INFORMATION

Keywords:
Jensen-alpha divergence
Dempster-Shafer theory
belief entropy
uncertainty modeling
fault diagnosis

DOI: 10.23967/j.rimni.2025.10.74645

SCIPEDIA Revista Internacional de Métodos Numéricos para Cálculo y Diseño en Ingeniería

Revista Internacional Métodos numéricos para cálculo y diseño en ingeniería RIMNI

In cooperation with CIMNE

Multisensor Fault Diagnosis Leveraging Reinforced Evidential Jensen-Alpha Divergence under Dempster-Shafer Theory

Zhe Liu[1,2,3,*], Juan Liao[4], Lili Wang[5], Yulong Huang[1], Kai Liu[1,6], Himanshu Dhumras[7] and Wulfran Fendzi Mbasso[8,9,10]

[1]College of Mathematics and Computer, Xinyu University, Xinyu, 338004, China

[2]Jadara Research Center, Jadara University, Irbid, 21110, Jordan

[3]School of Computer Sciences, Universiti Sains Malaysia, Penang, 11800, Malaysia

[4]School of Big Data Engineering, Kaili University, Kaili, 556000, China

[5]School of Artificial Intelligence, Dongguan City University, Dongguan, 523000, China

[6]School of Transportation Engineering, East China Jiaotong University, Nanchang, 330013, China

[7]School of Management, Shanghai University, Shanghai, 200444, China

[8]Department of Biosciences, Saveetha School of Engineering, Saveetha Institute of Medical and Technical Sciences, Chennai, 602105, India

[9]Technology and Applied Sciences Laboratory, University of Douala, Douala, P.O. Box 8689, Cameroon

[10]Applied Science Research Center, Applied Science Private University, Amman, 11937, Jordan

ABSTRACT

Uncertainty and conflicting information are pervasive in artificial intelligence (AI)-driven engineering systems, especially in multisensor fault diagnosis. Dempster-Shafer theory (DST) has garnered significant interest across various fields as it provides a powerful framework for modeling uncertainty. However, despite its advantages, the application of Dempster's rule can lead to paradoxical outcomes when it encounters highly conflicting evidence. To address this limitation, this paper first presents a new evidential Jensen-alpha divergence ($\mathcal{EJAD}$) to quantify the discrepancy between the evidence items based on DST. Furthermore, an advanced version, the reinforced evidential Jensen-alpha divergence ($\mathcal{REJAD}$) is developed, which takes into account the quantity of potential propositions. We demonstrate that $\mathcal{REJAD}$ can be transformed into various divergences such as the χ^2 divergence, Jensen-Shannon divergence, Hellinger distance, and arithmetic-geometric divergence under certain conditions. Also, we show the key properties of $\mathcal{REJAD}$, including non-negativity, non-degeneracy and symmetry. Additionally, we design a new multisensor fault diagnosis method utilizing $\mathcal{REJAD}$ and belief entropy. The superior performance of the proposed method is tested in three distinct fault diagnosis cases, and analysis shows robust performance across a range of its key parameter α, offering a computationally feasible, scalable and interpretable solution for AI-based decision-making in real-world engineering applications.

OPEN ACCESS

Received: 15/10/2025

Accepted: 17/11/2025

Published: 20/03/2026

DOI
10.23967/j.rimni.2025.10.74645

Keywords:
Jensen-alpha divergence
Dempster-Shafer theory
belief entropy
uncertainty modeling
fault diagnosis

*Correspondence: Zhe Liu (liuzhe921@gmail.com).

1 Introduction

The integration of artificial intelligence (AI) into engineering systems has led to significant advancements in intelligent fault diagnosis, which plays a crucial role in ensuring system safety, efficiency, and reliability [1–3]. AI-enabled applications such as predictive maintenance, real-time condition monitoring, and autonomous decision-making require accurate interpretation of sensor data, often collected from heterogeneous sources in complex environments. However, these systems frequently encounter challenges arising from uncertain, imprecise, or conflicting information, which can severely impact diagnostic accuracy and system robustness [4,5]. As such, effective uncertainty and imprecision modeling and data fusion methods are indispensable for enabling trustworthy AI in engineering contexts.

With the rapid advancement of information technologies and the increasing ease of data acquisition, multisensor fault diagnosis has garnered extensive attention in both academic research and engineering practice [6,7]. This area involves capturing diverse data from multiple sensors and platforms and integrating them to generate more accurate and comprehensive information [5,8]. However, integrating heterogeneous sensor data in complex, uncertain environments remains a formidable challenge. To address these issues, several theoretical frameworks have been proposed, including Dempster-Shafer theory (DST) [4,9], fuzzy set theory [10–12], complex evidence theory [13,14], and rough set theory [15,16].

Dempster-Shafer theory (DST) [17,18] is a mathematical framework for reasoning and modeling under uncertainty and imprecision, which has been successfully applied in various domains, including but not limited in pattern recognition [19,20], fault diagnosis [21–23] and information fusion [24–26]. Unlike classical probability theory, which relies on precise probabilities, DST represents uncertain and imprecise knowledge through mass functions or basic belief assignments (BBAs). Moreover, Dempster's rule offers a flexible method for combining evidence from multiple sources, enabling the integration of information with varying reliability and granularity. This makes DST particularly useful in applications requiring a comprehensive understanding of complex phenomena.

However, Dempster's rule can produce counterintuitive results when there is significant conflict about evidence items, exposing a limitation in the rule's applicability for certain cases where evidence combination may not align with common-sense reasoning [27,28]. To address this issue, extensive research has been conducted, primarily falling into two categories. The first category involves modifying Dempster's rule itself, with notable approaches including Dubois and Prade's disjunctive combination rule [29], Smets's unnormalized combination rule [30], and Yager's alternative combination rule [31]. While these modifications are innovative, they often compromise essential properties of Dempster's original formulation, such as associativity and commutativity, and have limited success in handling complex uncertainty with highly conflicting evidence, thus still risking counterintuitive outcomes. In light of the challenges presented, many scholars have gravitated towards preprocessing evidence as a viable solution pathway. Among these methods, Murphy's [32] method stands out for its simplicity, opting to average the evidence arithmetically. Alternatively, Deng et al. [33] introduced a method that calculates a weighted average based on the Jousselme distance, a strategy aiming to refine the integration of evidence. Jiang [34] suggested a correlation coefficient tailored to BBAs, thus enriching the discourse with a fresh perspective on evidence analysis. Xiao [35] took the discourse further by introducing a new belief divergence measure that also incorporates the concept of information volume and belief entropy, paving the way for a nuanced evaluation of evidence. Following this, Zhao et al. [36,37] explored divergence measures grounded in harmonic and square means,

offering innovative strategy to evidence assessment. Meanwhile, Kaur and Srivastava [38] proposed leveraging a logarithmic function-based divergence, aiming to enhance evidence analysis.

Despite the notable progress, several limitations persist in existing divergence-based methods. First, many methods [35–38] reduce multiple subsets into singletons in order to simplify the computation of the discrepancy between evidence items. While this improves tractability, it leads to a significant loss of semantic richness and structural information inherent in the original BBAs, which is especially detrimental in applications involving complex hypothesis spaces. Second, some methods [33,34,39] primarily assess the reliability of evidence based on factors such as credibility or uncertainty, without fully accounting for the internal diversity of BBAs or the relationships between focal elements. These limitations hinder their ability to effectively discriminate between similar but structurally distinct evidence items. Moreover, in scenarios with high degrees of conflict, many existing methods either fail to achieve meaningful consensus or excessively dilute the informational content in pursuit of consistency.

These unresolved challenges reveal an important research gap: current divergence measures in DST are often insufficiently sensitive to the underlying structural complexity and subset-level distinctions between BBAs. This shortcoming limits the effectiveness of evidence fusion, especially when dealing with heterogeneous sensors. To overcome these issues, this study proposes a novel divergence measure that incorporates both the discrepancy and the structural diversity of BBAs. In this way, it is intended to improve the reliability of evidence assessment and enhance the robustness of fault diagnosis under uncertain and conflicting conditions.

In this paper, we first introduce a new divergence measure, the evidential Jensen-alpha divergence ($\mathcal{EJAD}$), formulated within the framework of DST. To refine the ability to discern variations among different subsets accurately, we further propose the advanced version, the reinforced evidential Jensen-alpha divergence ($\mathcal{REJAD}$), which incorporates the consideration of the number of possible propositions, enhancing its appropriateness for quantifying the discrepancy between evidence items. Intriguingly, $\mathcal{REJAD}$ reverts to $\mathcal{EJAD}$ in scenarios where the BBA comprises solely singleton subsets. Finally, we present a $\mathcal{REJAD}$-based method for multisensor fault diagnosis in DST, demonstrating its applicability in handling complex data fusion scenarios. The main contributions of this work are summarized as follows:

1. A new divergence, named $\mathcal{REJAD}$, is presented to quantify the discrepancy between evidence items.
2. The properties of $\mathcal{REJAD}$ are thoroughly analyzed, which relates to the χ^2 divergence, Jensen-Shannon divergence, Hellinger distance and arithmetic-geometric divergence.
3. A new multisensor fault diagnosis method based on $\mathcal{REJAD}$ and belief entropy is developed. The performance of the proposed method has been tested by several fault diagnosis cases.

The rest arrangement of this paper is organized as follows: Section 2 briefly reviews the basics of DSTT. In Section 3, we propose the evidential Jensen-alpha divergence and its variants. Section 4 proposes a $\mathcal{REJAD}$-based multisensor fault diagnosis method. In Section 5, we verify the superiority of the proposed method on several fault diagnosis cases. Section 6 makes the conclusion.

2 Preliminaries

2.1 Dempster-Shafer Theory

Definition 1 (Framework of discernment): *Let* Λ *be a finite set of mutually exclusive and exhaustive elements, called the framework of discernment (FOD), which is denoted by:*

$$\Lambda = \{\lambda_1, \lambda_2, \cdots, \lambda_N\} \tag{1}$$

In DST, the power-set of Λ *is depicted as* 2^Λ:

$$2^\Lambda = \{\oslash, \{\lambda_1\}, \{\lambda_2\}, ..., \{\lambda_N\}, \{\lambda_1, \lambda_2\}, ..., \Lambda\} \tag{2}$$

where $\{\lambda_i\}$ *is the singleton subset,* $\{\lambda_i, \lambda_j\}$ *is the multiple subset and* $\oslash$ *is an empty set.*

Definition 2 (Mass function): *A mass function* $\mathbf{m}$, *also referred to as basic belief assignment (BBA), is a mapping from* 2^Λ *to* $[0, 1]$, *that assigns degrees of belief to subsets of FOD, and satisfies:*

$$\begin{cases} \sum\limits_{\lambda_i \subseteq \Lambda} m(\lambda_i) = 1 \\ m(\oslash) = 0 \end{cases} \tag{3}$$

where $m(\lambda_i) > 0$ *is called a focal element of* $\mathbf{m}$, *and* $m(\lambda_i)$ *denotes the mass of belief to* $\{\lambda_i\}$.

Definition 3 (Belief function): *For any focal element* $\{\lambda_i\}$, *the belief function* $Bel(\lambda_i)$ *is defined as:*

$$Bel(\lambda_i) = \sum_{\lambda_j \subseteq \lambda_i} m(\lambda_j) \tag{4}$$

Definition 4 (Plausibility function): *For any focal element* $\{\lambda_i\}$, *the plausibility function* $Pl(\lambda_i)$ *is defined as:*

$$Pl(\lambda_i) = \sum_{\lambda_j \cap \lambda_i \neq \oslash} m(\lambda_j) \tag{5}$$

where $Bel(\lambda_i)$ *and* $Pl(\lambda_i)$ *can be interpreted as the lower and upper bounds of the probability of* $\{\lambda_i\}$.

Definition 5 (Dempster's rule): *Given two mass functions* $\mathbf{m}_1$ *and* $\mathbf{m}_2$, *representing evidence from two different sources, the Dempster's rule is calculated as:*

$$m(\lambda_i) = \begin{cases} 0, & \lambda_i = \oslash \\ \dfrac{\sum\limits_{\lambda_j \cap \lambda_k = \lambda_i} m_1(\lambda_j) m_2(\lambda_k)}{1 - K}, & \lambda_i \neq \oslash \end{cases} \tag{6}$$

with

$$K = \sum_{\lambda_j \cap \lambda_k = \oslash} m_1(\lambda_j) m_2(\lambda_k) \tag{7}$$

where K *denotes the conflict coefficient between* $\mathbf{m}_1$ *and* $\mathbf{m}_2$.

2.2 Alpha Divergence Measure

Definition 6 (Alpha divergence): *Alpha divergence [40] is a crucial metric in information theory, used to quantify the discrepancy between two probability distributions. Its general formulation is defined as*

follows:

$$\mathcal{AD}(\mathcal{P},\mathcal{Q}) = \frac{\sum_i \left(p_i^{\alpha} q_i^{1-\alpha} - \alpha p_i + (\alpha-1)\, q_i\right)}{\alpha\,(\alpha-1)} \tag{8}$$

where $\mathcal{P}$ and $\mathcal{Q}$ represent two probability distributions, and $\alpha \in \mathbf{R} \setminus \{0,1\}$ is the divergence parameter, which can be tuned to derive various well-known divergences in specific cases. However, alpha divergence does not satisfy symmetry.

3 Proposed Alpha Divergence Measure

Although alpha divergence offers a robust means for comparing two probability distributions, applying it directly within the framework of DST presents challenges, particularly in accurately measuring discrepancy between evidence items. To address this issue, we introduce the evidential Jensen-alpha divergence ($\mathcal{EJAD}$) as a solution. Furthermore, we propose a reinforced evidential Jensen-alpha divergence ($\mathcal{REJAD}$). Additionally, some numerical examples will be given to show the effectiveness of $\mathcal{REJAD}$.

Definition 7 (Evidential Jensen-alpha divergence): *Let $\mathbf{m}_1$ and $\mathbf{m}_2$ be two BBAs in Λ. Evidential Jensen-alpha divergence ($\mathcal{EJAD}$) between $\mathbf{m}_1$ and $\mathbf{m}_2$ is defined as:*

$$\begin{aligned}\mathcal{EJAD}(\mathbf{m}_1,\mathbf{m}_2) &= \frac{1}{2}\left[\mathcal{AD}\left(\mathbf{m}_1, \frac{\mathbf{m}_1+\mathbf{m}_2}{2}\right) + \mathcal{AD}\left(\mathbf{m}_2, \frac{\mathbf{m}_1+\mathbf{m}_2}{2}\right)\right] \\ &= \frac{1}{2}\left[\frac{\sum\limits_{\lambda_i\subseteq\Lambda} m_1(\lambda_i)^{\alpha}\left(\frac{m_1(\lambda_i)+m_2(\lambda_i)}{2}\right)^{1-\alpha} - \alpha m_1(\lambda_i) + (\alpha-1)\frac{m_1(\lambda_i)+m_2(\lambda_i)}{2}}{\alpha(\alpha-1)}\right. \\ &\quad \left. + \frac{\sum\limits_{\lambda_i\subseteq\Lambda} m_2(\lambda_i)^{\alpha}\left(\frac{m_1(\lambda_i)+m_2(\lambda_i)}{2}\right)^{1-\alpha} - \alpha m_2(\lambda_i) + (\alpha-1)\frac{m_1(\lambda_i)+m_2(\lambda_i)}{2}}{\alpha(\alpha-1)}\right]\end{aligned} \tag{9}$$

where $\alpha \in \mathbf{R} \setminus \{0,1\}$.

Obviously, $\mathcal{EJAD}$ builds upon the traditional $\mathcal{AD}$ while adhering to principles of symmetry. Nonetheless, its ability to effectively measure multiple subsets is limited. Particularly, BBA is capable of not only assessing the quality of singleton subsets but also that of multiple subsets simultaneously. Once involves multiple subsets, it contains inherent uncertainty and imprecision that needs to be accounted for in the formula. Consequently, a Reinforced evidential Jensen-α divergence is introduced to address the limitation.

Definition 8 (Reinforced evidential Jensen-alpha divergence): *Let $\mathbf{m}_1$ and $\mathbf{m}_2$ be two BBAs in FOD Λ, where λ_i is a hypothesis of $\mathbf{m}$ and Λ contains mutually exclusive and exhaustive elements. Reinforced evidential Jensen-alpha divergence ($\mathcal{REJAD}$) between $\mathbf{m}_1$ and $\mathbf{m}_2$ is defined as:*

$$\mathcal{REJAD}(\mathbf{m}_1,\mathbf{m}_2)=\frac{1}{2}\left[\mathcal{AD}\left(\mathbf{m}_1,\frac{\mathbf{m}_1+\mathbf{m}_2}{2}\right)+\mathcal{AD}\left(\mathbf{m}_2,\frac{\mathbf{m}_1+\mathbf{m}_2}{2}\right)\right]$$
$$=\frac{1}{2}\left[\frac{\sum_{\lambda_i\subseteq\Lambda}\mathbb{M}_1(\lambda_i)^{\alpha}\left(\frac{\mathbb{M}_1(\lambda_i)+\mathbb{M}_2(\lambda_i)}{2}\right)^{1-\alpha}-\alpha\mathbb{M}_1(\lambda_i)+(\alpha-1)\frac{\mathbb{M}_1(\lambda_i)+\mathbb{M}_2(\lambda_i)}{2}}{\alpha(\alpha-1)}\right.$$
$$\left.+\frac{\sum_{\lambda_i\subseteq\Lambda}\mathbb{M}_2(\lambda_i)^{\alpha}\left(\frac{\mathbb{M}_1(\lambda_i)+\mathbb{M}_2(\lambda_i)}{2}\right)^{1-\alpha}-\alpha\mathbb{M}_2(\lambda_i)+(\alpha-1)\frac{\mathbb{M}_1(\lambda_i)+\mathbb{M}_2(\lambda_i)}{2}}{\alpha(\alpha-1)}\right] \tag{10}$$

where $\alpha\in\mathbf{R}\setminus\{0,1\}$ *and*

$$\mathbb{M}(\lambda_i)=\frac{m(\lambda_i)}{2^{|\lambda_i|}-1} \tag{11}$$

In (10), each belief mass $m(\lambda_i)$ is divided by a cardinality, denoted as $2^{|\lambda_i|}-1$, which accounts for all feasible combinations of λ_i, excluding the empty set. $\mathcal{REJAD}$ diverges from the conventional $\mathcal{AD}$ found in probability theory, where DST allows for the inclusion of multiple subsets within a single element. Moreover, $\mathcal{REJAD}$ extends the scope of $\mathcal{EJAD}$, providing a more comprehensive measure. Importantly, it is highlighted that when $|\lambda_i|=1$, and a BBA converges to a probability distribution, $\mathcal{REJAD}$ seamlessly transitions into $\mathcal{EJAD}$.

Remark 1: *Complexity of* $\mathcal{REJAD}$ *The calculation of* $\mathcal{REJAD}$ *between two BBAs* $\mathbf{m}_1$ *and* $\mathbf{m}_2$ *is primarily governed by the number of focal elements in the power set of the frame of discernment,* 2^{Λ}. *Let* $N=|\Lambda|$ *be the number of elements in the FOD. The maximum number of possible focal elements (non-empty subsets) is therefore* $X=|2^{\Lambda}|-1=2^N-1$. *However, in practical applications, BBAs are typically sparse—meaning mass is assigned only to a limited number of focal elements. Let* x *represent the number of focal elements with non-zero mass in the union of* $\mathbf{m}_1$ *and* $\mathbf{m}_2$, *where* $x\ll X$ *in most real-world scenarios.*

For two BBAs, the calculation of $\mathcal{REJAD}$ *as defined in (10) involves the following steps for each focal element* $\lambda_i\subseteq\Lambda$ *with non-zero mass in either BBA:*

- *Computing the transformed mass* $\mathbb{M}(\lambda_i)$ *using (11), which is an* $O(1)$ *operation per focal element.*
- *Evaluating the core alpha divergence terms in (10), involving exponentiation and multiplication operations that are* $O(1)$ *per focal element.*

Since these operations must be performed for each of the x *relevant focal elements, the overall time complexity for calculating* $\mathcal{REJAD}(\mathbf{m}_1,\mathbf{m}_2)$ *is* $O(x)$. *In the worst case where BBAs assign mass to all possible focal elements,* $x=X=2^N-1$, *resulting in exponential complexity. However, the sparse nature of practical BBAs makes* $O(x)$ *a more realistic characterization.*

Property 1: *Let* $\mathbf{m}_1$ *and* $\mathbf{m}_2$ *be two BBAs in* Λ, *some interesting properties of* $\mathcal{REJAD}$ *as follows:*

1. *When $\alpha = 2$, $\mathcal{REJAD}$ represents evidential χ^2 divergence ($\mathcal{E}\chi^2\mathcal{D}$):*

$$\mathcal{REJAD}(\mathbf{m}_1, \mathbf{m}_2) = \frac{1}{4}\mathcal{E}\chi^2\mathcal{D}(\mathbf{m}_1, \mathbf{m}_2) \tag{12}$$

where

$$\mathcal{E}\chi^2\mathcal{D}(\mathbf{m}_1, \mathbf{m}_2) = \sum_{\lambda_i \subseteq \Lambda} \frac{(\mathbb{M}_1(\lambda_i) - \mathbb{M}_2(\lambda_i))^2}{\mathbb{M}_1(\lambda_i) + \mathbb{M}_2(\lambda_i)} \tag{13}$$

2. *When $\alpha \to 1$, $\mathcal{REJAD}$ degenerates to evidential Jensen-Shannon divergence ($\mathcal{EJSD}$):*

$$\mathcal{REJAD}(\mathbf{m}_1, \mathbf{m}_2) = \frac{1}{2}\mathcal{EJSD}(\mathbf{m}_1, \mathbf{m}_2) \tag{14}$$

where

$$\mathcal{EJSD}(\mathbf{m}_1, \mathbf{m}_2) = \sum_{\lambda_i \subseteq \Lambda} \mathbb{M}_1(\lambda_i) \ln \frac{2\mathbb{M}_1(\lambda_i)}{\mathbb{M}_1(\lambda_i) + \mathbb{M}_2(\lambda_i)} + \mathbb{M}_2(\lambda_i) \ln \frac{2\mathbb{M}_2(\lambda_i)}{\mathbb{M}_1(\lambda_i) + \mathbb{M}_2(\lambda_i)} \tag{15}$$

3. *$\alpha = \frac{1}{2}$, $\mathcal{REJAD}$ simplifies into evidential Hellinger distance ($\mathcal{EHD}$):*

$$\mathcal{REJAD}(\mathbf{m}_1, \mathbf{m}_2) = \mathcal{EHD}(\mathbf{m}_1, \mathbf{m}_2) \tag{16}$$

where

$$\begin{aligned} \mathcal{EHD}(\mathbf{m}_1, \mathbf{m}_2) = &\sum_{\lambda_i \subseteq \Lambda} \left(\sqrt{\mathbb{M}_1(\lambda_i)} - \sqrt{\frac{\mathbb{M}_1(\lambda_i) + \mathbb{M}_2(\lambda_i)}{2}} \right)^2 \\ &+ \sum_{\lambda_i \subseteq \Lambda} \left(\sqrt{\mathbb{M}_2(\lambda_i)} - \sqrt{\frac{\mathbb{M}_1(\lambda_i) + \mathbb{M}_2(\lambda_i)}{2}} \right)^2 \end{aligned} \tag{17}$$

4. *When $\alpha \to 0$, $\mathcal{REJAD}$ degenerates to the symmetric evidential arithmetic-geometric divergence ($\mathcal{EAGD}$):*

$$\mathcal{REJAD}(\mathbf{m}_1, \mathbf{m}_2) = \mathcal{EAGD}(\mathbf{m}_1, \mathbf{m}_2) \tag{18}$$

where

$$\mathcal{EAGD}(\mathbf{m}_1, \mathbf{m}_2) = \sum_{\lambda_i \subseteq \Lambda} \frac{\mathbb{M}_1(\lambda_i) + \mathbb{M}_2(\lambda_i)}{2} \ln \frac{\mathbb{M}_1(\lambda_i) + \mathbb{M}_2(\lambda_i)}{2\sqrt{\mathbb{M}_1(\lambda_i)\mathbb{M}_2(\lambda_i)}} \tag{19}$$

5. *When $\alpha = -1$, $\mathcal{REJAD}$ degenerates to symmetric evidential χ^2 divergence ($\mathcal{SE}\chi^2\mathcal{D}$):*

$$\mathcal{REJAD}(\mathbf{m}_1, \mathbf{m}_2) = \frac{1}{16}\mathcal{SE}\chi^2\mathcal{D}(\mathbf{m}_1, \mathbf{m}_2) \tag{20}$$

where

$$\mathcal{SE}\chi^2\mathcal{D}(\mathbf{m}_1, \mathbf{m}_2) = \sum_{\lambda_i \subseteq \Lambda} \frac{(\mathbb{M}_1(\lambda_i) - \mathbb{M}_2(\lambda_i))^2 (\mathbb{M}_1(\lambda_i) + \mathbb{M}_2(\lambda_i))}{\mathbb{M}_1(\lambda_i)\mathbb{M}_2(\lambda_i)} \tag{21}$$

Proof: Let consider two BBAs $\mathbf{m}_1$ and $\mathbf{m}_2$ in Λ, some proofs as follows:

1. When $\alpha = 2$,

$$\mathcal{REJAD}(\mathbf{m}_1, \mathbf{m}_2) = \frac{1}{2}\left[\frac{\sum_{\lambda_i \subseteq \Lambda}\left(\mathbb{M}_1(\lambda_i)^2\left(\frac{\mathbb{M}_1(\lambda_i)+\mathbb{M}_2(\lambda_i)}{2}\right)^{-1} - 2\mathbb{M}_1(\lambda_i) + \frac{\mathbb{M}_1(\lambda_i)+\mathbb{M}_2(\lambda_i)}{2}\right)}{2}\right.$$
$$\left. + \frac{\sum_{\lambda_i \subseteq \Lambda}\left(\mathbb{M}_2(\lambda_i)^2\left(\frac{\mathbb{M}_1(\lambda_i)+\mathbb{M}_2(\lambda_i)}{2}\right)^{-1} - 2\mathbb{M}_2(\lambda_i) + \frac{\mathbb{M}_1(\lambda_i)+\mathbb{M}_2(\lambda_i)}{2}\right)}{2}\right]$$
$$= \frac{1}{4}\left[\sum_{\lambda_i \subseteq \Lambda}\left(\frac{2\mathbb{M}_1(\lambda_i)^2}{\mathbb{M}_1(\lambda_i)+\mathbb{M}_2(\lambda_i)} - 2\mathbb{M}_1(\lambda_i) + \frac{\mathbb{M}_1(\lambda_i)+\mathbb{M}_2(\lambda_i)}{2}\right.\right.$$
$$\left.\left. + \frac{2\mathbb{M}_2(\lambda_i)^2}{\mathbb{M}_1(\lambda_i)+\mathbb{M}_2(\lambda_i)} - 2\mathbb{M}_2(\lambda_i) + \frac{\mathbb{M}_1(\lambda_i)+\mathbb{M}_2(\lambda_i)}{2}\right)\right]$$
$$= \frac{1}{4}\left[\sum_{\lambda_i \subseteq \Lambda}\frac{2\left(\mathbb{M}_1(\lambda_i)^2 + \mathbb{M}_2(\lambda_i)^2\right) - \left(\mathbb{M}_1(\lambda_i)+\mathbb{M}_2(\lambda_i)\right)^2}{\mathbb{M}_1(\lambda_i)+\mathbb{M}_2(\lambda_i)}\right]$$
$$= \frac{1}{4}\left[\sum_{\lambda_i \subseteq \Lambda}\frac{\left(\mathbb{M}_1(\lambda_i)-\mathbb{M}_2(\lambda_i)\right)^2}{\mathbb{M}_1(\lambda_i)+\mathbb{M}_2(\lambda_i)}\right]$$
$$= \frac{1}{4}\mathcal{E}\chi^2\mathcal{D}(\mathbf{m}_1, \mathbf{m}_2)$$

2. When $\alpha \to 1$,

$$\lim_{\alpha\to 1}\mathcal{REJAD}(\mathbf{m}_1, \mathbf{m}_2)$$
$$= \lim_{\alpha\to 1}\frac{1}{2}\left[\frac{\frac{\partial}{\partial\alpha}\left(\sum_{\lambda_i \subseteq \Lambda}\mathbb{M}_1(\lambda_i)^\alpha\left(\frac{\mathbb{M}_1(\lambda_i)+\mathbb{M}_2(\lambda_i)}{2}\right)^{1-\alpha} - \alpha\mathbb{M}_1(\lambda_i) + (\alpha-1)\left(\frac{\mathbb{M}_1(\lambda_i)+\mathbb{M}_2(\lambda_i)}{2}\right)\right)}{\frac{\partial}{\partial\alpha}(\alpha(\alpha-1))}\right.$$
$$\left. + \frac{\frac{\partial}{\partial\alpha}\left(\sum_{\lambda_i \subseteq \Lambda}\mathbb{M}_2(\lambda_i)^\alpha\left(\frac{\mathbb{M}_1(\lambda_i)+\mathbb{M}_2(\lambda_i)}{2}\right)^{1-\alpha} - \alpha\mathbb{M}_2(\lambda_i) + (\alpha-1)\left(\frac{\mathbb{M}_1(\lambda_i)+\mathbb{M}_2(\lambda_i)}{2}\right)\right)}{\frac{\partial}{\partial\alpha}(\alpha(\alpha-1))}\right]$$
$$= \lim_{\alpha\to 1}\frac{1}{2}\left[\frac{\sum_{\lambda_i \subseteq \Lambda}\mathbb{M}_1(\lambda_i)^\alpha\left(\frac{\mathbb{M}_1(\lambda_i)+\mathbb{M}_2(\lambda_i)}{2}\right)^{1-\alpha}\ln\frac{2\mathbb{M}_1(\lambda_i)}{\mathbb{M}_1(\lambda_i)+\mathbb{M}_2(\lambda_i)} - \mathbb{M}_1(\lambda_i) + \left(\frac{\mathbb{M}_1(\lambda_i)+\mathbb{M}_2(\lambda_i)}{2}\right)}{2\alpha-1}\right.$$

$$+\frac{\sum_{\lambda_i\subseteq\Lambda}\mathbb{M}_2(\lambda_i)^{\alpha}\left(\frac{\mathbb{M}_1(\lambda_i)+\mathbb{M}_2(\lambda_i)}{2}\right)^{1-\alpha}\ln\frac{2\mathbb{M}_2(\lambda_i)}{\mathbb{M}_1(\lambda_i)+\mathbb{M}_2(\lambda_i)}-\mathbb{M}_2(\lambda_i)+\left(\frac{\mathbb{M}_1(\lambda_i)+\mathbb{M}_2(\lambda_i)}{2}\right)}{2\alpha-1}\Bigg]$$

$$=\frac{1}{2}\left[\sum_{\lambda_i\subseteq\Lambda}\left(\mathbb{M}_1(\lambda_i)\ln\frac{2\mathbb{M}_1(\lambda_i)}{\mathbb{M}_1(\lambda_i)+\mathbb{M}_2(\lambda_i)}+\mathbb{M}_2(\lambda_i)\ln\frac{2\mathbb{M}_2(\lambda_i)}{\mathbb{M}_1(\lambda_i)+\mathbb{M}_2(\lambda_i)}\right)\right]$$

$$=\frac{1}{2}\mathcal{EJSD}(\mathbf{m}_1,\mathbf{m}_2)$$

3. When $\alpha=\frac{1}{2}$,

$$\mathcal{REJAD}(\mathbf{m}_1,\mathbf{m}_2)=\frac{1}{2}\Bigg[\frac{\sum_{\lambda_i\subseteq\Lambda}\left(\mathbb{M}_1(\lambda_i)^{\frac{1}{2}}\left(\frac{\mathbb{M}_1(\lambda_i)+\mathbb{M}_2(\lambda_i)}{2}\right)^{\frac{1}{2}}-\frac{1}{2}\mathbb{M}_1(\lambda_i)-\frac{1}{2}\left(\frac{\mathbb{M}_1(\lambda_i)+\mathbb{M}_2(\lambda_i)}{2}\right)\right)}{-\frac{1}{4}}$$

$$+\frac{\sum_{\lambda_i\subseteq\Lambda}\left(\mathbb{M}_2(\lambda_i)^{\frac{1}{2}}\left(\frac{\mathbb{M}_1(\lambda_i)+\mathbb{M}_2(\lambda_i)}{2}\right)^{\frac{1}{2}}-\frac{1}{2}\mathbb{M}_2(\lambda_i)-\frac{1}{2}\left(\frac{\mathbb{M}_1(\lambda_i)+\mathbb{M}_2(\lambda_i)}{2}\right)\right)}{-\frac{1}{4}}\Bigg]$$

$$=\frac{1}{2}\Bigg[2\sum_{\lambda_i\subseteq\Lambda}\left(\sqrt{\mathbb{M}_1(\lambda_i)}-\sqrt{\frac{\mathbb{M}_1(\lambda_i)+\mathbb{M}_2(\lambda_i)}{2}}\right)^2$$

$$+2\sum_{\lambda_i\subseteq\Lambda}\left(\sqrt{\mathbb{M}_2(\lambda_i)}-\sqrt{\frac{\mathbb{M}_1(\lambda_i)+\mathbb{M}_2(\lambda_i)}{2}}\right)^2\Bigg]$$

$$=\sum_{\lambda_i\subseteq\Lambda}\left(\sqrt{\mathbb{M}_1(\lambda_i)}-\sqrt{\frac{\mathbb{M}_1(\lambda_i)+\mathbb{M}_2(\lambda_i)}{2}}\right)^2$$

$$+\sum_{\lambda_i\subseteq\Lambda}\left(\sqrt{\mathbb{M}_{\mathbf{m}_2}(\lambda_i)}-\sqrt{\frac{\mathbb{M}_{\mathbf{m}_1}(\lambda_i)+\mathbb{M}_{\mathbf{m}_2}(\lambda_i)}{2}}\right)^2$$

$$=\mathcal{EHD}(\mathbf{m}_1,\mathbf{m}_2)$$

4. When $\alpha\to 0$,

$$\lim_{\alpha\to 0}\mathcal{REJAD}(\mathbf{m}_1,\mathbf{m}_2)$$

$$=\lim_{\alpha\to 0}\frac{1}{2}\Bigg[\frac{\frac{\partial}{\partial\alpha}\left(\sum_{\lambda_i\subseteq\Lambda}\left(\mathbb{M}_1(\lambda_i)^{\alpha}\left(\frac{\mathbb{M}_1(\lambda_i)+\mathbb{M}_2(\lambda_i)}{2}\right)^{1-\alpha}-\alpha\mathbb{M}_1(\lambda_i)+(\alpha-1)\left(\frac{\mathbb{M}_1(\lambda_i)+\mathbb{M}_2(\lambda_i)}{2}\right)\right)\right)}{\frac{\partial}{\partial\alpha}(\alpha(\alpha-1))}$$

$$+\frac{\frac{\partial}{\partial\alpha}\left(\sum_{\lambda_i\subseteq\Lambda}\left(\mathbb{M}_2(\lambda_i)^{\alpha}\left(\frac{\mathbb{M}_1(\lambda_i)+\mathbb{M}_2(\lambda_i)}{2}\right)^{1-\alpha}-\alpha\mathbb{M}_2(\lambda_i)+(\alpha-1)\left(\frac{\mathbb{M}_1(\lambda_i)+\mathbb{M}_2(\lambda_i)}{2}\right)\right)\right)}{\frac{\partial}{\partial\alpha}\left(\alpha(\alpha-1)\right)}\Bigg]$$

$$=\lim_{\alpha\to 0}\frac{1}{2}\Bigg[\frac{\sum_{\lambda_i\subseteq\Lambda}\left(\mathbb{M}_1(\lambda_i)^{\alpha}\left(\frac{\mathbb{M}_1(\lambda_i)+\mathbb{M}_2(\lambda_i)}{2}\right)^{1-\alpha}\ln\frac{2\mathbb{M}_1(\lambda_i)}{\mathbb{M}_1(\lambda_i)+\mathbb{M}_2(\lambda_i)}-\mathbb{M}_1(\lambda_i)+\frac{\mathbb{M}_1(\lambda_i)+\mathbb{M}_2(\lambda_i)}{2}\right)}{2\alpha-1}$$

$$+\frac{\sum_{\lambda_i\subseteq\Lambda}\left(\mathbb{M}_2(\lambda_i)^{\alpha}\left(\frac{\mathbb{M}_1(\lambda_i)+\mathbb{M}_2(\lambda_i)}{2}\right)^{1-\alpha}\ln\frac{2\mathbb{M}_2(\lambda_i)}{\mathbb{M}_1(\lambda_i)+\mathbb{M}_2(\lambda_i)}-\mathbb{M}_2(\lambda_i)+\frac{\mathbb{M}_1(\lambda_i)+\mathbb{M}_2(\lambda_i)}{2}\right)}{2\alpha-1}\Bigg]$$

$$=\frac{1}{2}\left[\frac{\sum_{\lambda_i\subseteq\Lambda}\left(\frac{\mathbb{M}_1(\lambda_i)+\mathbb{M}_2(\lambda_i)}{2}\ln\frac{2\mathbb{M}_1(\lambda_i)}{\mathbb{M}_1(\lambda_i)+\mathbb{M}_2(\lambda_i)}+\frac{\mathbb{M}_1(\lambda_i)+\mathbb{M}_2(\lambda_i)}{2}\ln\frac{2\mathbb{M}_2(\lambda_i)}{\mathbb{M}_1(\lambda_i)+\mathbb{M}_2(\lambda_i)}\right)}{-1}\right]$$

$$=\frac{1}{2}\left[-\sum_{\lambda_i\subseteq\Lambda}\frac{\mathbb{M}_1(\lambda_i)+\mathbb{M}_2(\lambda_i)}{2}\ln\frac{4\mathbb{M}_1(\lambda_i)\mathbb{M}_2(\lambda_i)}{\left(\mathbb{M}_1(\lambda_i)+\mathbb{M}_2(\lambda_i)\right)^2}\right]$$

$$=\sum_{\lambda_i\subseteq\Lambda}\frac{\mathbb{M}_1(\lambda_i)+\mathbb{M}_2(\lambda_i)}{2}\ln\frac{\mathbb{M}_1(\lambda_i)+\mathbb{M}_2(\lambda_i)}{2\sqrt{\mathbb{M}_1(\lambda_i)\mathbb{M}_1(\lambda_i)}}$$

$$=\mathcal{EAGD}(\mathbf{m}_1,\mathbf{m}_2)$$

5. When $\alpha=-1$,

$$\mathcal{REJAD}(\mathbf{m}_1,\mathbf{m}_2)=\frac{1}{2}\Bigg[\frac{\sum_{\lambda_i\subseteq\Lambda}\left(\mathbb{M}_1(\lambda_i)^{-1}\left(\frac{\mathbb{M}_1(\lambda_i)+\mathbb{M}_2(\lambda_i)}{2}\right)^2+\mathbb{M}_1(\lambda_i)-\left(\mathbb{M}_1(\lambda_i)+\mathbb{M}_2(\lambda_i)\right)\right)}{2}$$

$$+\frac{\sum_{\lambda_i\subseteq\Lambda}\left(\mathbb{M}_2(\lambda_i)^{-1}\left(\frac{\mathbb{M}_1(\lambda_i)+\mathbb{M}_2(\lambda_i)}{2}\right)^2+\mathbb{M}_2(\lambda_i)-\left(\mathbb{M}_1(\lambda_i)+\mathbb{M}_2(\lambda_i)\right)\right)}{2}\Bigg]$$

$$=\frac{1}{2}\left[\frac{\sum_{\lambda_i\subseteq\Lambda}\left(\frac{\left(\mathbb{M}_1(\lambda_i)+\mathbb{M}_2(\lambda_i)\right)^2}{4\mathbb{M}_1(\lambda_i)}-\mathbb{M}_2(\lambda_i)\right)}{2}\right]$$

$$+\frac{\sum_{\lambda_i\subseteq\Lambda}\left(\frac{\left(\mathbb{M}_1(\lambda_i)+\mathbb{M}_2(\lambda_i)\right)^2}{4\mathbb{M}_2(\lambda_i)}-\mathbb{M}_1(\lambda_i)\right)}{2}\Bigg]$$

$$=\frac{1}{2}\left[\frac{\sum_{\lambda_i\subseteq\Lambda}\frac{\left(\mathbb{M}_1(\lambda_i)-\mathbb{M}_2(\lambda_i)\right)^2}{4\mathbb{M}_1(\lambda_i)}}{2}+\frac{\sum_{\lambda_i\subseteq\Lambda}\frac{\left(\mathbb{M}_1(\lambda_i)-\mathbb{M}_2(\lambda_i)\right)^2}{4\mathbb{M}_2(\lambda_i)}}{2}\right]$$

$$=\frac{1}{16}\left[\sum_{\lambda_i\subseteq\Lambda}\frac{\left(\mathbb{M}_1(\lambda_i)-\mathbb{M}_2(\lambda_i)\right)^2\left(\mathbb{M}_1(\lambda_i)+\mathbb{M}_2(\lambda_i)\right)}{\mathbb{M}_1(\lambda_i)\mathbb{M}_2(\lambda_i)}\right]$$

$$=\frac{1}{16}\mathcal{SE}\chi^2\mathcal{D}(\mathbf{m}_1,\mathbf{m}_2)\ \square$$

Property 2: *Some outstanding properties can be given based on the above special cases:*

1. *Nonnegativity:* $\mathcal{REJAD}(\mathbf{m}_1,\mathbf{m}_2)\geq 0$.
2. *Nondegeneracy:* $\mathcal{REJAD}(\mathbf{m}_1,\mathbf{m}_2)=0$ *if* $\mathbf{m}_1{=}\mathbf{m}_2$.
3. *Symmetry:* $\mathcal{REJAD}(\mathbf{m}_1,\mathbf{m}_2)=\mathcal{REJAD}(\mathbf{m}_2,\mathbf{m}_1)$.

These properties are suitable for assessing the level of conflict and discrepancy between evidence items. Next, several examples are used to illustrate the properties of $\mathcal{REJAD}$.

Example 1: *Suppose* $\mathbf{m}_1$ *and* $\mathbf{m}_2$ *are two BBAs in* $\Lambda=\{\lambda_1,\lambda_2\}$.

$\mathbf{m}_1$: $m_1(\{\lambda_1\})=x,\ \ m_1(\{\lambda_2\})=y,\ \ m_1(\{\lambda_1,\lambda_2\})=1-x-y$

$\mathbf{m}_2$: $m_2(\{\lambda_1\})=y,\ \ m_2(\{\lambda_2\})=x,\ \ m_2(\{\lambda_1,\lambda_2\})=1-x-y$

where $x,y,x+y\in[0,1]$.

As illustrated in Fig. 1, we take $\alpha=2$, *the variations in* x *and* y *induce symmetric alterations in* $\mathbf{m}_1$ *and* $\mathbf{m}_2$. *Meanwhile, the values of* $\mathcal{E}\chi^2\mathcal{D}$ *remain steady, illustrating the natural symmetry of* $\mathcal{E}\chi^2\mathcal{D}$. *This finding is in harmony with the anticipated symmetry property of* $\mathcal{E}\chi^2\mathcal{D}$. *Moreover, no matter how* x *and* y *take values,* $\mathcal{E}\chi^2\mathcal{D}$ *is always greater than or equal to 0, which also proves nonnegativity.*

Example 2: *Suppose two BBAs* $\mathbf{m}_1$ *and* $\mathbf{m}_2$ *in* Λ, *where* x *is a variable with a value between 0 and 1, and* Λ_T *represents a variable subset where the number of elements, as shown in Table 1.*

$\mathbf{m}_1$: $m_1(\{\lambda_2\})=x, m_1(\Lambda_T)=1-x$

$\mathbf{m}_2$: $m_2(\{\lambda_2\})=0.8, m_2(\Lambda_T)=0.2$

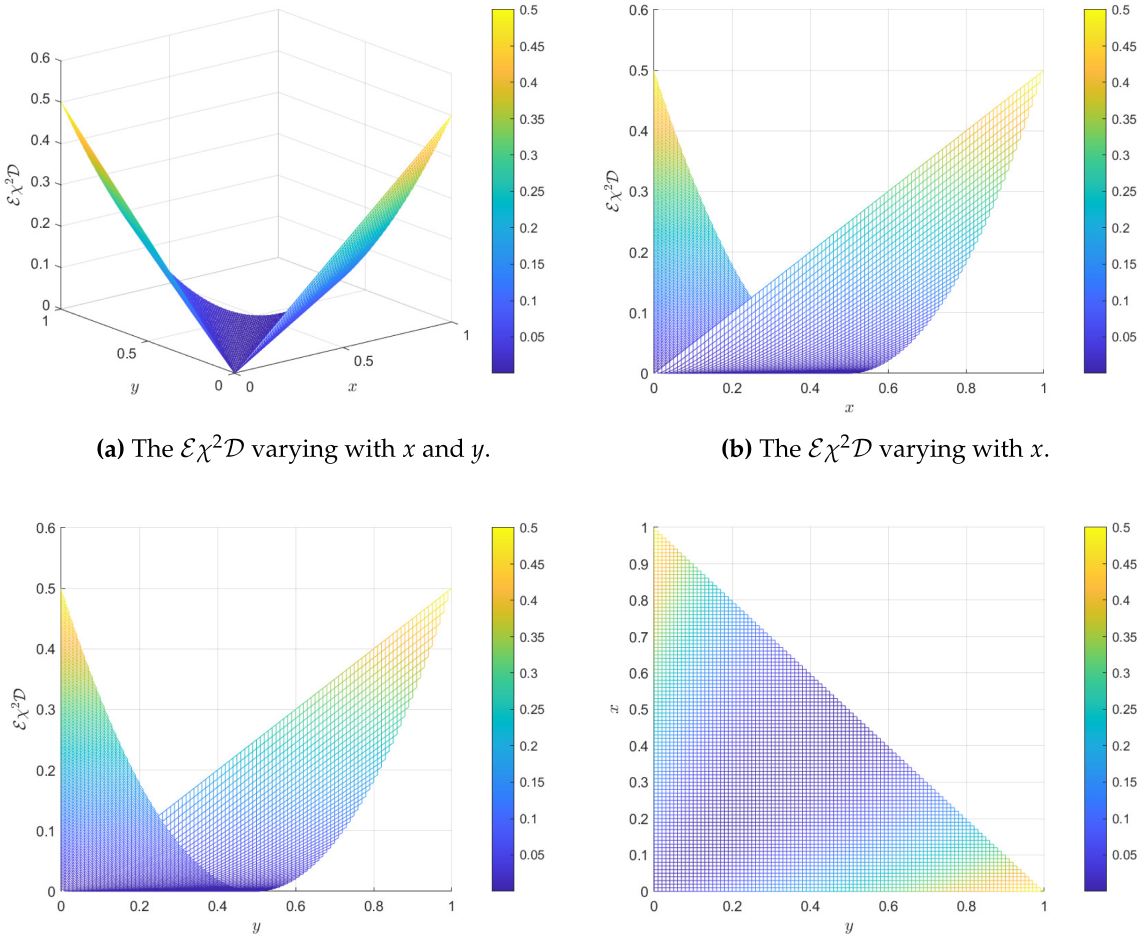

(a) The $\mathcal{E}\chi^2\mathcal{D}$ varying with x and y.

(b) The $\mathcal{E}\chi^2\mathcal{D}$ varying with x.

(c) The $\mathcal{E}\chi^2\mathcal{D}$ varying with y.

(d) Variation of x and y.

Figure 1: The values of $\mathcal{E}\chi^2\mathcal{D}$ varying with x and y in Example 1 (a–d)

Table 1: Variable set T_V

t	T_V
1	$\{\lambda_1\}$
2	$\{\lambda_1, \lambda_2\}$
3	$\{\lambda_1, \lambda_2, \lambda_3\}$
4	$\{\lambda_1, \lambda_2, \lambda_3, \lambda_4\}$
5	$\{\lambda_1, \lambda_2, \lambda_3, \lambda_4, \lambda_5\}$
6	$\{\lambda_1, \lambda_2, \lambda_3, \lambda_4, \lambda_5, \lambda_6\}$
7	$\{\lambda_1, \lambda_2, \lambda_3, \lambda_4, \lambda_5, \lambda_6, \lambda_7\}$
8	$\{\lambda_1, \lambda_2, \lambda_3, \lambda_4, \lambda_5, \lambda_6, \lambda_7, \lambda_8\}$
9	$\{\lambda_1, \lambda_2, \lambda_3, \lambda_4, \lambda_5, \lambda_6, \lambda_7, \lambda_8, \lambda_9\}$
10	$\{\lambda_1, \lambda_2, \lambda_3, \lambda_4, \lambda_5, \lambda_6, \lambda_7, \lambda_8, \lambda_9, \lambda_{10}\}$

(Continued)

Table 1 (continued)

t	T_V
11	$\{\lambda_1, \lambda_2, \lambda_3, \lambda_4, \lambda_5, \lambda_6, \lambda_7, \lambda_8, \lambda_9, \lambda_{10}, \lambda_{11}\}$
12	$\{\lambda_1, \lambda_2, \lambda_3, \lambda_4, \lambda_5, \lambda_6, \lambda_7, \lambda_8, \lambda_9, \lambda_{10}, \lambda_{11}, \lambda_{12}\}$
13	$\{\lambda_1, \lambda_2, \lambda_3, \lambda_4, \lambda_5, \lambda_6, \lambda_7, \lambda_8, \lambda_9, \lambda_{10}, \lambda_{11}, \lambda_{12}, \lambda_{13}\}$
14	$\{\lambda_1, \lambda_2, \lambda_3, \lambda_4, \lambda_5, \lambda_6, \lambda_7, \lambda_8, \lambda_9, \lambda_{10}, \lambda_{11}, \lambda_{12}, \lambda_{13}, \lambda_{14}\}$
15	$\{\lambda_1, \lambda_2, \lambda_3, \lambda_4, \lambda_5, \lambda_6, \lambda_7, \lambda_8, \lambda_9, \lambda_{10}, \lambda_{11}, \lambda_{12}, \lambda_{13}, \lambda_{14}, \lambda_{15}\}$
16	$\{\lambda_1, \lambda_2, \lambda_3, \lambda_4, \lambda_5, \lambda_6, \lambda_7, \lambda_8, \lambda_9, \lambda_{10}, \lambda_{11}, \lambda_{12}, \lambda_{13}, \lambda_{14}, \lambda_{15}, \lambda_{16}\}$
17	$\{\lambda_1, \lambda_2, \lambda_3, \lambda_4, \lambda_5, \lambda_6, \lambda_7, \lambda_8, \lambda_9, \lambda_{10}, \lambda_{11}, \lambda_{12}, \lambda_{13}, \lambda_{14}, \lambda_{15}, \lambda_{16}, \lambda_{17}\}$
18	$\{\lambda_1, \lambda_2, \lambda_3, \lambda_4, \lambda_5, \lambda_6, \lambda_7, \lambda_8, \lambda_9, \lambda_{10}, \lambda_{11}, \lambda_{12}, \lambda_{13}, \lambda_{14}, \lambda_{15}, \lambda_{16}, \lambda_{17}, \lambda_{18}\}$
19	$\{\lambda_1, \lambda_2, \lambda_3, \lambda_4, \lambda_5, \lambda_6, \lambda_7, \lambda_8, \lambda_9, \lambda_{10}, \lambda_{11}, \lambda_{12}, \lambda_{13}, \lambda_{14}, \lambda_{15}, \lambda_{16}, \lambda_{17}, \lambda_{18}, \lambda_{19}\}$
20	$\{\lambda_1, \lambda_2, \lambda_3, \lambda_4, \lambda_5, \lambda_6, \lambda_7, \lambda_8, \lambda_9, \lambda_{10}, \lambda_{11}, \lambda_{12}, \lambda_{13}, \lambda_{14}, \lambda_{15}, \lambda_{16}, \lambda_{17}, \lambda_{18}, \lambda_{19}, \lambda_{20}\}$

The relationship between $\mathcal{EJSD}$, x and t is illustrated in Fig. 2. Specifically, as $t = 1$, indicating Λ_T is a singleton set, there is no imprecise information, leading to an increase in $\mathcal{EJSD}$ value. As we expand the size of Λ_T from 2 to 20, a decreasing trend in $\mathcal{EJSD}$ values is observable, as depicted in Fig. 2c. This decrease is attributed to the exponential growth in uncertainty and imprecision with more elements. Regarding x, at $x = 0.8$ where $\mathbf{m}_1 = \mathbf{m}_2$, $\mathcal{EJSD}$ reaches its minimum value of 0 regardless of t variations. Therefore, we verify the property of nondegeneracy.

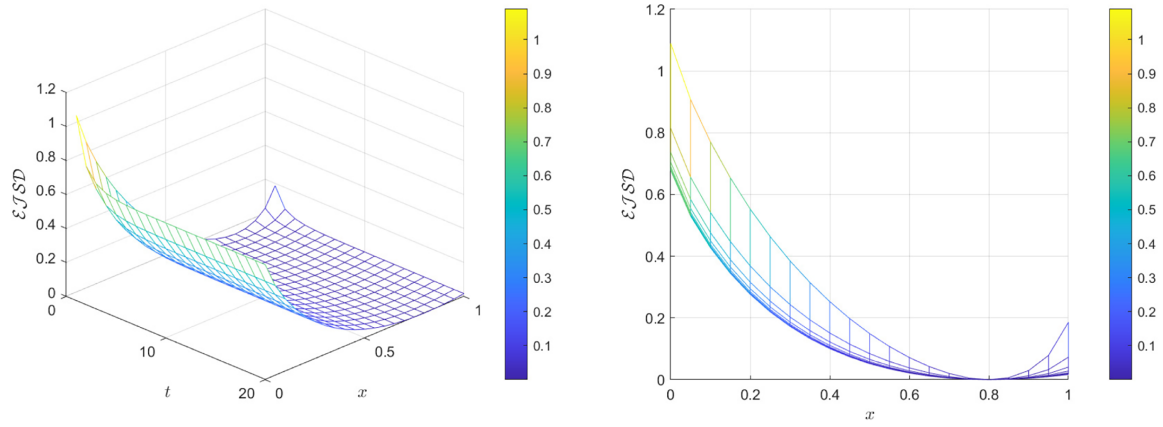

(a) The $\mathcal{EJSD}$ varying with x and t.

(b) The $\mathcal{EJSD}$ varying with x.

Figure 2: (Continued)

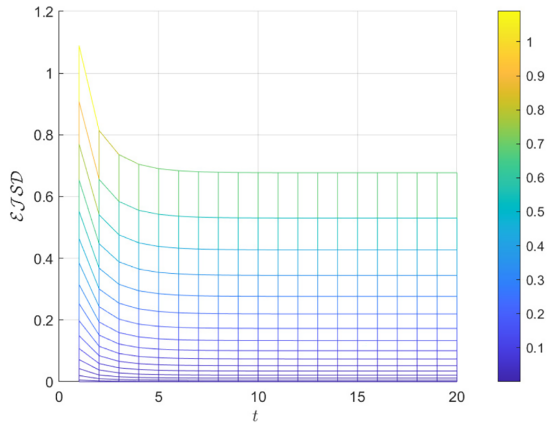

(c) The $\mathcal{EJSD}$ varying with t.

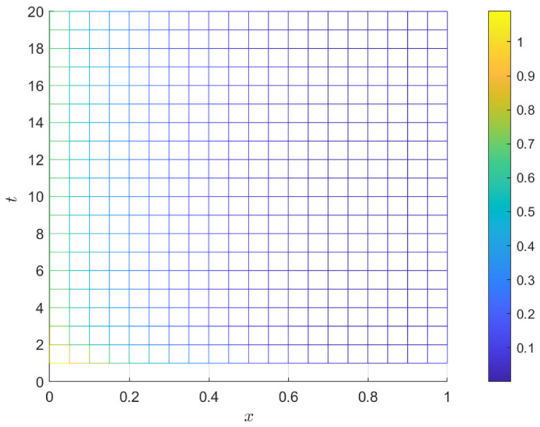

(d) Variation of x and t.

Figure 2: The values of $\mathcal{EJSD}$ varying with x and t in example 2 (a–d)

Example 3: *Suppose two BBAs* $\mathbf{m}_1$ *and* $\mathbf{m}_2$ *in* Λ, *where* x *is a variable with a value between 0 and 1, and* Λ_T *represents a variable subset where the number of elements, as shown in Table 1.*

$\mathbf{m}_1$: $m_1(\{\lambda_1, \lambda_2, \lambda_3\}) = x, m_1(\Lambda_T) = 1 - x$

$\mathbf{m}_2$: $m_2(\{\lambda_1, \lambda_2, \lambda_3\}) = 0.8, m_2(\Lambda_T) = 0.2$

where $x \in [0, 1]$ *and* $T_V \in \{1, 2, ..., 20\}$.

As $\alpha = 1/2$ *leading to the* $\mathcal{EHD}$. *Fig. 3 exhibits similarities to Example 2 overall. Nonetheless, the presence of multiple elements within the subset results in a decreased* $\mathcal{EHD}$ *value. This scenario underscores the efficacy of* $\mathcal{EHD}$ *in contexts where subsets consist of several elements, illustrating its robust performance under these conditions.*

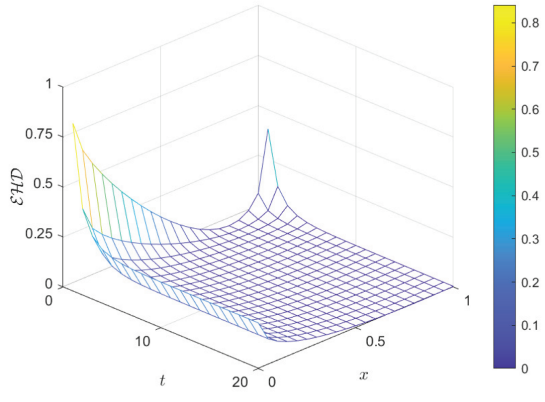

(a) The $\mathcal{EHD}$ varying with x and t.

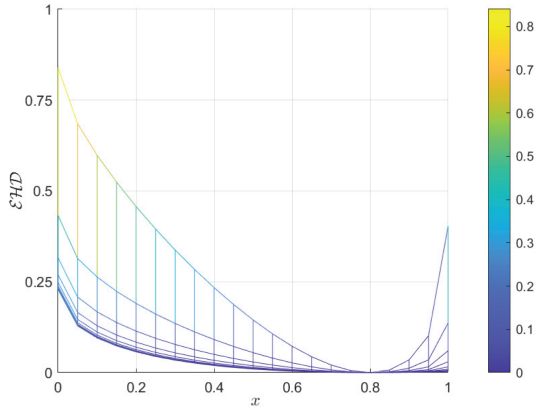

(b) The $\mathcal{EHD}$ varying with t.

Figure 3: (Continued)

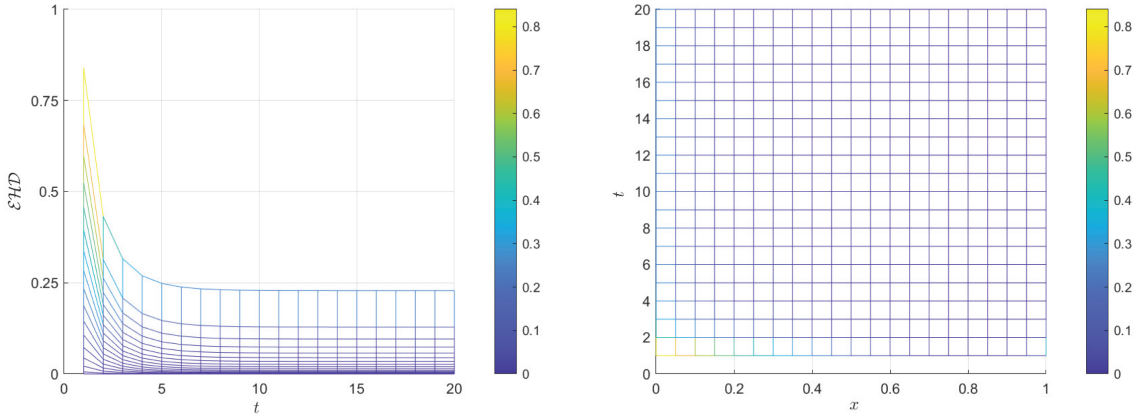

(c) The $\mathcal{EHD}$ varying with x.

(d) Variation of x and t.

Figure 3: The values of $\mathcal{EHD}$ varying with x and t in example 3 (a–d)

4 $\mathcal{REJAD}$-Based Multisenor Fault Diagnosis Method

In this section, we introduce a new method to multisensor data fusion based on the DST. The proposed method encompasses a more sophisticated fusion strategy by incorporating $\mathcal{REJAD}$ and belief entropy, aiming to handle uncertainty and imprecision skillfully. In particular, $\mathcal{REJAD}$ is employed as a measure to evaluate the discrepancy between the evidence items, especially useful in conflicting evidence. This allows for the allocation of reduced weight to conflicting evidence and greater weight to harmonious evidence. Furthermore, belief entropy [4] is utilized to assess the uncertainty inherent in each evidence. The proposed method stands on a solid theoretical foundation and is equally viable for practical applications. The flowchart of the proposed multisensor fault diagnosis method is illustrated in Fig. 4. The steps for the proposed method are described as follows:

Let us consider p independent evidence items $\mathbf{m}_k$ $(k = 1, \cdots, p)$ on $\Lambda = \{\lambda_1, \cdots, \lambda_N\}$.

Step 1: The divergence, $\mathcal{REJAD}$, between two evidence items $\mathbf{m}_k$ $(k = 1, 2, \cdots, p)$ and $\mathbf{m}_l$ $(l = 1, 2, \cdots, p)$ is computed using (10). Afterwards, one can assemble the divergence measure matrix (DMM) as follows:

$$DMM = \begin{bmatrix} 0 & \cdots & \mathcal{REJAD}_{1k} & \cdots & \mathcal{REJAD}_{1p} \\ \vdots & \ddots & \vdots & & \vdots \\ \mathcal{REJAD}_{l1} & \cdots & 0 & \cdots & \mathcal{REJAD}_{lN} \\ \vdots & & \vdots & \ddots & \vdots \\ \mathcal{REJAD}_{p1} & \cdots & \mathcal{REJAD}_{pk} & \cdots & 0 \end{bmatrix} \tag{22}$$

Step 2: Calculate the average divergence from DMM, denoted as $\mathcal{RE}\tilde{\mathcal{J}}\mathcal{AD}_k$. The formula is expressed as:

$$\mathcal{RE}\tilde{\mathcal{J}}\mathcal{AD}_k = \frac{\sum_{\substack{l=1 \\ l \neq k}}^{p} \mathcal{REJAD}_{kl}}{p-1} \tag{23}$$

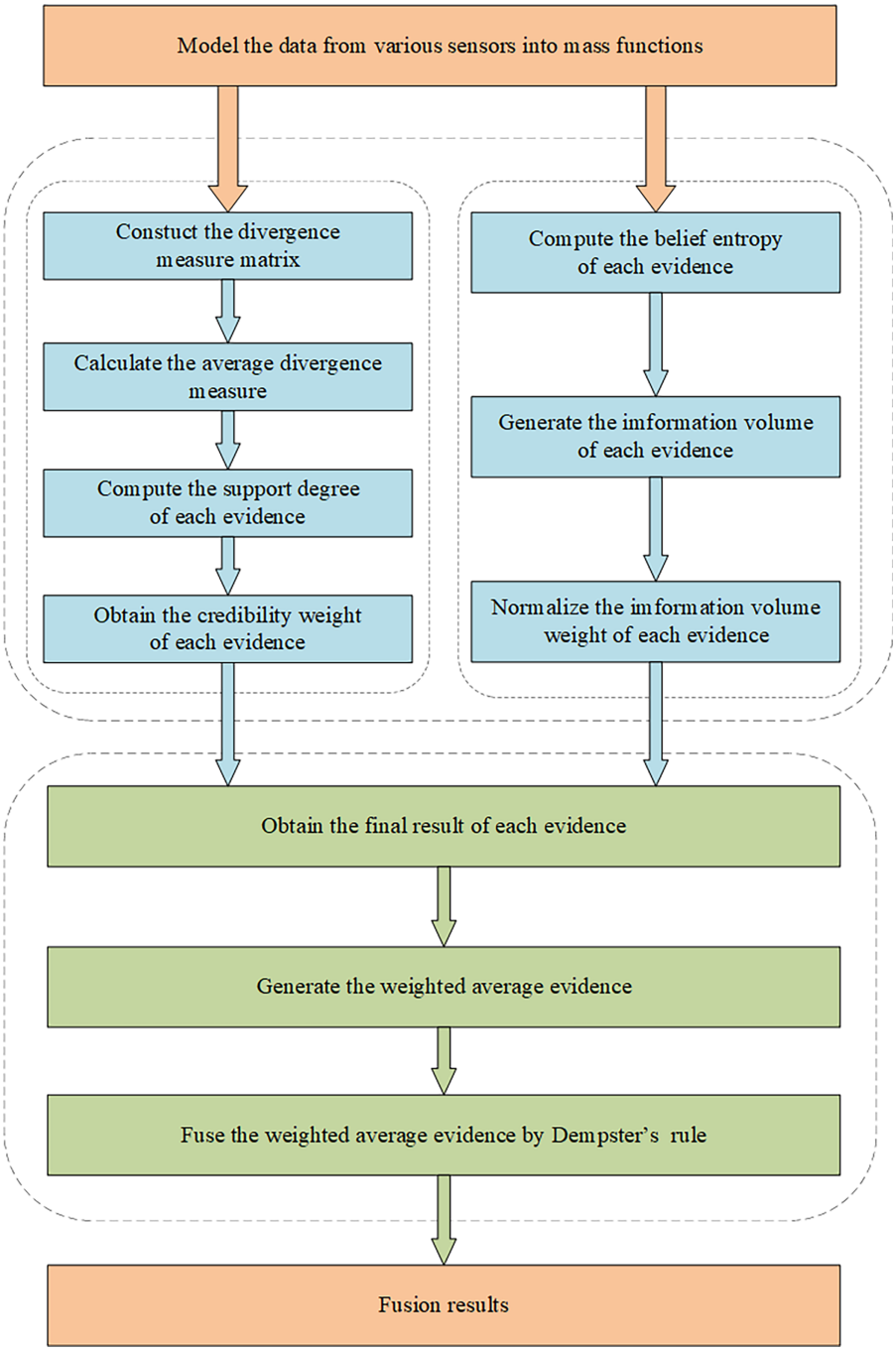

Figure 4: The flowchart of the proposed multisensor fault diagnosis method

Step 3: The support degree of evidence $\mathbf{m}_k$ is determined using the following calculation:

$$SD_k = \frac{1}{\mathcal{RE}\tilde{\mathcal{J}}\mathcal{AD}_k} \tag{24}$$

Step 4: The credibility degree Crd_k of m_k is defined by the ensuing formula:

$$Crd_k = \frac{SD_k}{\sum_{k=1}^{p} SD_k} \tag{25}$$

Step 5: The belief entropy for $\mathbf{m}_k$, denoted as E_k, is computed as follows:

$$E_k = \sum_{\lambda_i \in \Lambda} \mathcal{BPL}_{\mathbf{m}_k}(\lambda_i) \log_2 \left(\frac{1}{\mathcal{BPL}_{\mathbf{m}_k}(\lambda_i)} \right) + \sum_{\lambda_i \subseteq \Lambda} m_k(\lambda_i) \log_2(2^{|\lambda_i|} - 1) \tag{26}$$

where

$$\mathcal{BPL}(\lambda_i) = \frac{Bel(\lambda_i) + Pl(\lambda_i)}{\sum_{\lambda_i \in \Lambda} Bel(\lambda_i) + Pl(\lambda_i)} \tag{27}$$

Step 6: In order to prevent the assignment of non-contributory weights to $\mathbf{m}_k$, the information volume IV_k is delineated as follows:

$$IV_k = \exp(E_k), \quad \forall k = 1, \ldots, p \tag{28}$$

Step 7: Proceed to standardize the information volume, which is symbolized by $\tilde{IV}_k$:

$$\tilde{IV}_k = \frac{IV_k}{\sum_{k=1}^{p} IV_k} \tag{29}$$

Step 8: Calculate the final weight $A\tilde{C}rd_k$:

$$A\tilde{C}rd_k = \frac{Crd_k \times \tilde{IV}_k}{\sum_{k=1}^{p} Crd_k \times \tilde{IV}_k} \tag{30}$$

Step 9: Compute the weighted average evidence $\tilde{\mathbf{m}}$ as follows:

$$\tilde{\mathbf{m}} = \sum_{k=1}^{p} A\tilde{C}rd_k \times \mathbf{m}_k \tag{31}$$

Step 10: Utilizing Dempster's rule, aggregate the weighted evidence $\tilde{\mathbf{m}}p - 1$ times as below:

$$R(\tilde{\mathbf{m}}) = \tilde{\mathbf{m}} \oplus \tilde{\mathbf{m}} \oplus \ldots \oplus \tilde{\mathbf{m}} \tag{32}$$

where $R(\tilde{\mathbf{m}})$ is the final combination result.

Remark 2: *Complexity of the proposed fusion method The overall complexity of the proposed fusion method depends on both the number of sensors p and the sparsity parameter x.*

- ***Step 1:*** *This step requires pairwise calculation of $\mathcal{RESJAD}$ for all p sensors. The number of unique pairwise comparisons is $p(p-1)/2 \approx O(p^2)$. Since each pairwise divergence calculation is $O(x)$, the complexity of this step is $O(k \cdot p^2)$.*
- ***Steps 2–4, 6–8:*** *These steps involve aggregating values from the DMM and performing arithmetic operations for each of the p sensors. Their complexities are dominated by $O(p^2)$ (from summing rows of the DMM) and $O(p)$, which is subsumed by the $O(x \cdot p^2)$ term from Step 1.*
- ***Step 5:*** *Calculating the belief entropy E_k for each of the p sensors involves processing each focal element in the BBA, resulting in complexity: $O(x \cdot p)$.*

- ***Step 9:*** *Computing the weighted average evidence* $\hat{\mathbf{m}}$ *involves a linear combination of* p *BBAs, with complexity:* $O(x \cdot p)$
- ***Step 10:*** *Combining the weighted average evidence* $\hat{\mathbf{m}}$ $p-1$ *times using Dempster's rule has considerable complexity. A naive implementation of Dempster's rule for two BBAs has complexity* $O(x^2)$*, leading to an overall complexity of approximately:* $O(x^2 \cdot p)$ *for* $p-1$ *sequential combinations.*

The overall time complexity of the fusion method combines the dominant terms from the analysis above: $O(x \cdot p^2 + x^2 \cdot p)$.

This analysis reveals that the method scales polynomially with respect to the number of sensors p*, while being sensitive to the sparsity and number of focal elements* x.

- *For systems with a fixed and small* N *(e.g.,* $N \leq 5$*), the method can efficiently handle a large number of sensors.*
- *When the hypothesis space is large (*$N > 10$*), the sparsity of BBAs (*$x \ll X$*) becomes crucial for practical implementation.*
- *For applications requiring real-time performance with large N, approximation techniques such as confining beliefs to a subset of hypotheses (e.g., only singletons and two-element subsets) can be employed to limit* x.

Here, we illustrate the implementation of the proposed method through an example.

Example 4: *Consider five distinct types of sensors in* $\Theta = \{\lambda_1, \lambda_2, \lambda_3\}$*, illustrated in Table 2.*

Table 2: BBAs in Example 4

BBAs	$\{\lambda_1\}$	$\{\lambda_2\}$	$\{\lambda_3\}$	$\{\lambda_2, \lambda_3\}$	$\{\lambda_1, \lambda_2\}$	Λ
$\mathbf{m}_1$	0.5	0.1	0.1	0.1	0.05	0.15
$\mathbf{m}_2$	0.2	0.3	0	0.4	0	0.1
$\mathbf{m}_3$	0.4	0.1	0.1	0.1	0	0.3
$\mathbf{m}_4$	0.7	0	0.05	0	0	0.25
$\mathbf{m}_5$	0	0.3	0.5	0	0.1	0.1

Step 1: *Construct the divergence measure matrix DMM as follows:*

$$DMM = \begin{bmatrix} 0 & 0.1162 & 0.0104 & 0.0655 & 0.2856 \\ 0.1162 & 0 & 0.0976 & 0.2434 & 0.3004 \\ 0.0104 & 0.0976 & 0 & 0.0713 & 0.2644 \\ 0.0655 & 0.2434 & 0.0713 & 0 & 0.4673 \\ 0.2856 & 0.3004 & 0.2644 & 0.4673 & 0 \end{bmatrix}$$

Step 2: *Compute the average divergence* $\mathcal{RE}\tilde{\mathcal{J}}\mathcal{AD}_k$:

$\mathcal{RE}\tilde{\mathcal{J}}\mathcal{AD}_1 = 0.1194,$

$\mathcal{RE}\tilde{\mathcal{J}}\mathcal{AD}_2 = 0.1894,$

$\mathcal{RE}\tilde{\mathcal{J}}\mathcal{AD}_3 = 0.1109,$

$\mathcal{RE}\tilde{\mathcal{J}}\mathcal{AD}_4 = 0.2119,$

$\mathcal{RE}\tilde{\mathcal{J}}\mathcal{AD}_5 = 0.3294$

Step 3: *Calculate the support degree* SD_k of $\mathbf{m}_k$:

$SD_1 = 8.3741,$

$SD_2 = 5.2796,$

$SD_3 = 9.0144,$

$SD_4 = 4.7191,$

$SD_5 = 3.0357$

Step 4: *Calculate the credibility degree* Crd_k of $\mathbf{m}_k$:

$Crd_1 = 0.2753,$

$Crd_2 = 0.1735,$

$Crd_3 = 0.2963,$

$Crd_4 = 0.1551,$

$Crd_5 = 0.0998$

Step 5: *Generate the belief entropy* E_k of $\mathbf{m}_k$:

$E_1 = 2.0545,$

$E_2 = 2.1364,$

$E_3 = 2.4747,$

$E_4 = 1.7998,$

$E_5 = 1.6401$

Step 6: *Measure the information volume* IV_k of $\mathbf{m}_k$:

$IV_1 = 7.8031,$

$IV_2 = 8.4690,$

$IV_3 = 11.8787,$

$IV_4 = 6.0483,$

$IV_5 = 5.1559$

Step 7: *Obtain the normalized information volume* $\tilde{IV}_k$ of $\mathbf{m}_k$:

$\tilde{IV}_1 = 0.1983,$

$\tilde{IV}_2 = 0.2152,$

$\tilde{IV}_3 = 0.3018,$

$\tilde{IV}_4 = 0.1537,$

$\tilde{IV}_5 = 0.1310$

Step 8: *Obtain the final weight* $\tilde{ACrd}_k$:

$\tilde{ACrd}_1 = 0.2500,$

$\tilde{ACrd}_2 = 0.1711,$

$\tilde{ACrd}_3 = 0.4097,$

$\tilde{ACrd}_4 = 0.1092,$

$\tilde{ACrd}_5 = 0.0599$

Step 9: *Obtain the weighted average evidence* $\tilde{\mathbf{m}}$:

$\tilde{m}(\{\lambda_1\}) = 0.3996,$

$\tilde{m}(\{\lambda_2\}) = 0.1353,$

$\tilde{m}(\{\lambda_3\}) = 0.1014,$

$\tilde{m}(\{\lambda_1, \lambda_2\}) = 0.1344,$

$\tilde{m}(\{\lambda_2, \lambda_3\}) = 0.0185,$

$\tilde{m}(\Theta) = 0.2108$

Step 10: *Utilize Dempster's rule to amalgamate the weighted average evidence (denoted as* $\tilde{m}$*) a total of four times. The outcomes of these combinations are presented in Table 3 and Fig. 5, where they are juxtaposed with results from other methods to highlight the differences.*

Table 3: Results with different methods in Example 4

Methods	$\{\lambda_1\}$	$\{\lambda_2\}$	$\{\lambda_3\}$	$\{\lambda_1, \lambda_2\}$	$\{\lambda_2, \lambda_3\}$	Λ
Dempster's rule [17]	0.6350	0.3050	0.0365	0.0187	0.0031	0.0018
Murphy's method [32]	0.7837	0.1634	0.0360	0.0143	0.0014	0.0012
Deng et al.'s method [33]	0.8394	0.1225	0.0218	0.0140	0.0011	0.0012
Lin et al's method [6]	0.8213	0.1352	0.0268	0.0142	0.0012	0.0013
Jiang's method [34]	0.8513	0.1150	0.0174	0.0143	0.0010	0.0012
Kaur and Srivastava's method [38]	0.8050	0.1472	0.0313	0.0140	0.0013	0.0012
Proposed method$^{(2)}$	0.8660	0.1013	0.0129	0.0173	0.0008	0.0016

(Continued)

Table 3 (continued)

Methods	$\{\lambda_1\}$	$\{\lambda_2\}$	$\{\lambda_3\}$	$\{\lambda_1, \lambda_2\}$	$\{\lambda_2, \lambda_3\}$	Λ
Proposed method$^{(1)}$	0.8675	0.0998	0.0128	0.0174	0.0008	0.0016
Proposed method$^{(1/2)}$	0.8699	0.0974	0.0128	0.0173	0.0008	0.0017
Proposed method$^{(0)}$	0.8756	0.0917	0.0129	0.0171	0.0009	0.0018
Proposed method$^{(-1)}$	0.8718	0.0942	0.0117	0.0196	0.0007	0.0020

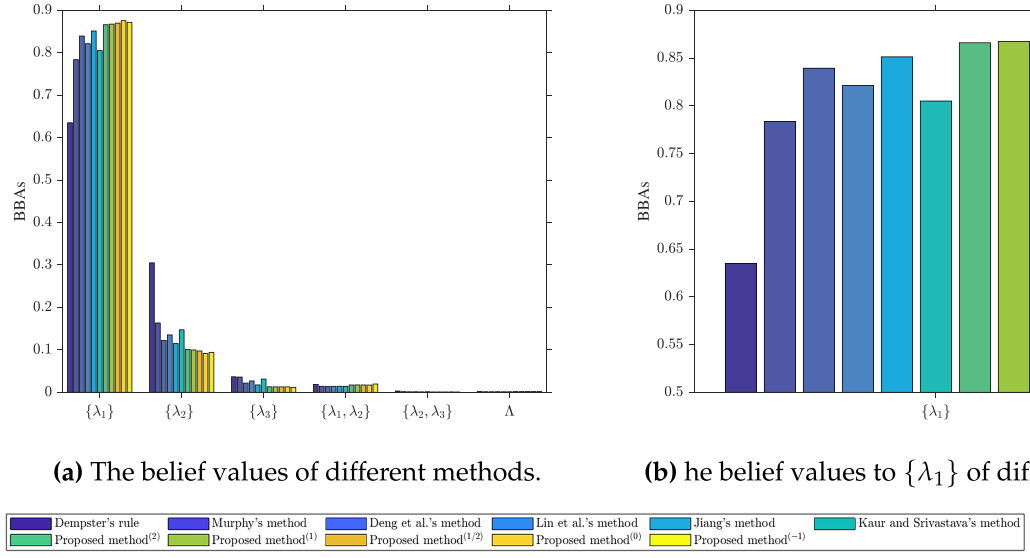

(a) The belief values of different methods. **(b)** he belief values to $\{\lambda_1\}$ of different methods.

Figure 5: Results with different methods (a,b) [6,17,32,33,34]

The analysis of Table 2 reveals that the evidence items $\mathbf{m}_1$, $\mathbf{m}_3$ *and* $\mathbf{m}_4$ *endorse* $\{\lambda_1\}$ *as the true target, indicating a consensus on its identification. In contrast,* $\mathbf{m}_2$ *offers a more equivocal stance regarding the identity of the target, while* $\mathbf{m}_5$ *distinctly identifies* $\{\lambda_3\}$ *as the target, starkly diverging from the consensus and creating notable discord among the evidence items. Such discord, particularly pronounced in evidence* $\mathbf{m}_5$*, along with the ambiguity introduced by* $\mathbf{m}_2$*, effectively muddles the overall clarity on the true target. To enhance the reality of the fusion outcome, it is prudent to de-emphasize these evidence items by assigning them lower weight factors during the final fusion process.*

Table 3 and Fig. 5 demonstrate that while all methods accurately identify the actual target, the belief degree of their identification varies. Dempster's rule [17] faces challenges in delivering satisfactory outcomes amidst conflicting evidence scenarios. Murphy's [32] averaging strategy tends to smooth over the distinctions among pieces of evidence, potentially overlooking critical differences. Conversely, the methods by Deng et al.'s [33] and Jiang's [34] focus on the discrepancy between evidence items but overlook the inherent uncertainty within each evidence. While Lin et al.'s [6] method and Kaur and Srivastava's [38] method yield plausible results, they neglect the interaction between different subsets. The proposed method can accurately identify the target, demonstrating significant performance improvements over alternative methods. As depicted in Fig. 5b, the belief masses for the target $\{\lambda_1\}$ *assigned by different*

methods highlight the superior efficacy of the proposed method in real-world decision-making contexts, attributed mainly to its enhanced identification accuracy.

5 Application in Multisensor Fault Diagnosis

In this section, we demonstrate the effectiveness of our proposed method through its application in real-world fault diagnosis scenarios. By examining three distinct cases of fault diagnosis, we showcase the superior performance of the proposed method.

5.1 Fault Diagnosis of Motor Rotor

In the context of diagnosing faults in motor rotors, three distinct sensor types are employed to gather characteristic data on acceleration, velocity, and displacement. The information acquired from these sensors is then converted into BBAs, which are comprehensively detailed in [34]. Table 4 illustrates that $\mathbf{m}_1$, $\mathbf{m}_2$ and $\mathbf{m}_3$ correspond to the evidence items derived from the acceleration sensor, velocity sensor, and displacement sensor, respectively. Typically, a motor rotor can be in one of four states: $\{\lambda_0\}$ indicating normal operation, $\{\lambda_1\}$ signifying unbalance, $\{\lambda_2\}$ denoting misalignment, and $\{\lambda_3\}$ representing pedestal looseness. Consequently, a frame of discernment, Λ, is established, encompassing these states: $\{\lambda_0, \lambda_1, \lambda_2, \lambda_3\}$. This framework facilitates the systematic analysis of the rotor condition based on the evidence collected from the various sensors.

Table 4: BBAs in fault diagnosis of motor rotor

BBAs	$\{\lambda_0\}$	$\{\lambda_1\}$	$\{\lambda_2\}$	$\{\lambda_3\}$	Λ
$\mathbf{m}_1$	0.06	0.68	0.02	0.04	0.20
$\mathbf{m}_2$	0.02	0	0.79	0.05	0.14
$\mathbf{m}_3$	0.02	0.58	0.16	0.04	0.20

Upon analyzing the three evidence items, it is obvious that the second evidence diverges significantly from the others. This difference suggests that while the majority of the evidence supports the state of $\{\lambda_2\}$, indicating unbalance, the second evidence points towards a different diagnosis, specifically misalignment. This inconsistency underscores the need for careful consideration and potentially the application of reconciliation measures or weighted analysis to address the conflicting evidence and arrive at a more accurate diagnosis of the condition of the motor rotor.

In this case, a decision-making threshold of 0.7 is implemented, consistent with the benchmarking practice established in the prior literature [34]. As illustrated in Table 5 and Fig. 6, the employments of Dempster's rule [17], Murphy's method [32], and Kaur and Srivastava's method [38] to merge these three evidence items did not significantly enhance the accuracy of decisions. Conversely, while both the proposed method and comparative techniques [6,33,34] pinpoint state λ_1 as the anomaly, ours delivers superior judgment accuracy. Furthermore, the application of different α values in our method consistently results in superior performance compared to related methods. This scenario effectively demonstrates the effectiveness of the proposed method in conflict resolution, thereby underlining the applicability of the proposed method in pertinent situations.

Table 5: Comparisons of different methods

Methods	$\{\lambda_0\}$	$\{\lambda_1\}$	$\{\lambda_2\}$	$\{\lambda_3\}$	Λ	Fault type
Dempster's rule [17]	0.0205	0.5230	0.3933	0.0309	0.0324	Uncertainty
Murphy's method [32]	0.0112	0.6059	0.3508	0.0153	0.0168	Uncertainty
Deng et al.'s method [41]	0.0111	0.7730	0.1856	0.0139	0.0165	$\{\lambda_1\}$
Lin et al's method [6]	0.0110	0.7019	0.2556	0.0147	0.0169	$\{\lambda_1\}$
Jiang's method [34]	0.0108	0.8063	0.1534	0.0134	0.0162	$\{\lambda_1\}$
Kaur and Srivastava's method [38]	0.0113	0.6487	0.3081	0.0151	0.0169	Uncertainty
Proposed method$^{(2)}$	0.0097	0.8516	0.1105	0.0124	0.0157	$\{\lambda_1\}$
Proposed method$^{(1)}$	0.0096	0.8523	0.1100	0.0124	0.0157	$\{\lambda_1\}$
Proposed method$^{(1/2)}$	0.0095	0.8541	0.1084	0.0124	0.0157	$\{\lambda_1\}$
Proposed method$^{(0)}$	0.0099	0.8618	0.1006	0.0122	0.0155	$\{\lambda_1\}$
Proposed method$^{(-1)}$	0.0096	0.8612	0.1014	0.0122	0.0156	$\{\lambda_1\}$

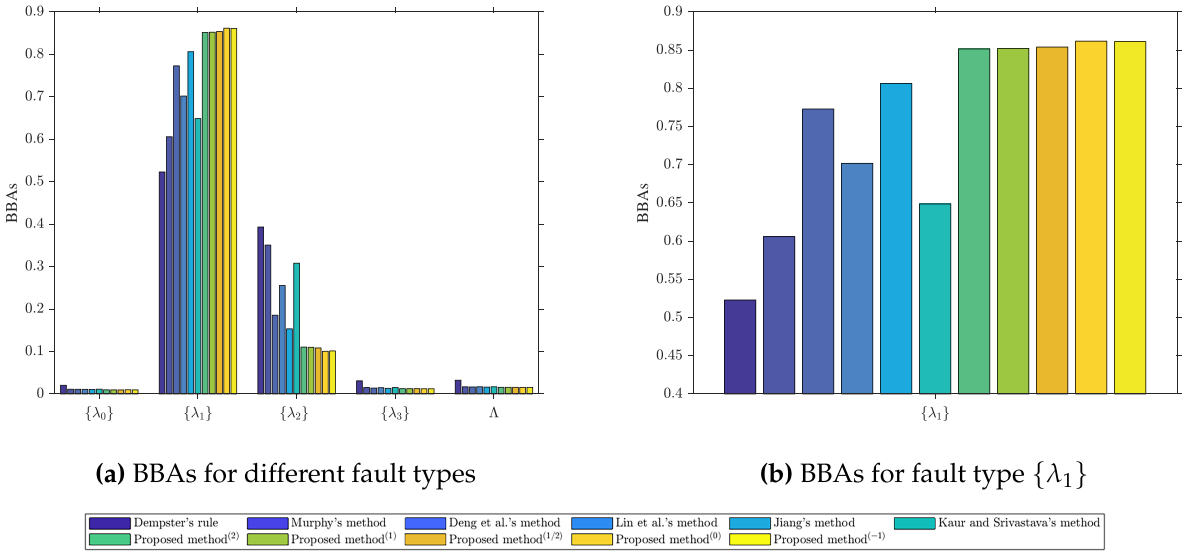

(a) BBAs for different fault types **(b)** BBAs for fault type $\{\lambda_1\}$

Figure 6: Results with different methods (a,b) [6,17,32,34,38,41]

5.2 Fault Diagnosis of Machines

In this subsection, we implement our method for a case study on machine fault diagnosis, as outlined in [35], to perform a comparative evaluation against existing methods. We establish a discernment framework, Λ, for identifying machine malfunctions, which includes three distinct fault types: $\Lambda = \{\lambda_1, \lambda_2, \lambda_3\}$. For the collection of diagnostic data, a trio of sensors are strategically placed on different machine components. The information acquired from these sensors is transformed into BBAs, with Table 6 offering an in-depth breakdown, where $\mathbf{m}_1, \mathbf{m}_2$ and $\mathbf{m}_3$ correspond to the BBAs generated by sensors, respectively.

Table 6: BBAs in fault diagnosis of machines

BBAs	$\{\lambda_1\}$	$\{\lambda_2\}$	$\{\lambda_2, \lambda_3\}$	Λ
$\mathbf{m}_1$	0.60	0.10	0.10	0.20
$\mathbf{m}_2$	0.05	0.80	0.05	0.10
$\mathbf{m}_3$	0.7	0.10	0.10	0.10

Additionally, to markedly improve the precision of our fault diagnosis method, we incorporate two distinct reliability indexes: Λ and τ, which can be established based on expert evaluations or empirical data, as shown in Table 7. The inclusion of Λ and τ is crucial for enhancing the accuracy of our diagnostic analysis, thereby guaranteeing more accurate and dependable conclusions in the fault identification process.

Table 7: Sufficiency and importance indexes of evidence

Parameters	$\mathbf{m}_1$	$\mathbf{m}_2$	$\mathbf{m}_3$
Sufficiency index: Λ	1.00	0.60	1.00
Importance index: τ	1.00	0.34	1.00

From Table 8, it is clear that Dempster's rule of combination encounters difficulties with conflicting evidence, mistakenly identifying the fault type as $\{\lambda_2\}$. In contrast, alternative methods, including our suggested method, adeptly navigate these inconsistencies. Our method, in particular, excels in accurately diagnosing fault type $\{\lambda_1\}$, achieving a belief degree of 0.8974—a performance that outstrips those of other methods, as shown in Fig. 7. This superior accuracy stems from the shortcomings of Murphy's method [32], along with the techniques proposed by Deng et al.'s [33], Lin et al.'s [6], Jiang's [34], and Kaur and Srivastava's [38] methods, which only take into account the differences between evidence items, and some methods cannot adequately differentiate between multiple subsets and singleton subsets, treating them as equivalent. Conversely, our method considers the diversity within subsets, making a clear distinction between multiple and single subsets. Furthermore, it employs belief entropy to measure the uncertainty of evidence. Such combined consideration establishes the superiority of the proposed method in effectively managing and interpreting conflicting evidence.

Table 8: Results of different methods

Methods	$\{\lambda_1\}$	$\{\lambda_2\}$	$\{\lambda_2, \lambda_3\}$	Λ	Fault type
Dempster's rule [17]	0.4519	0.5048	0.0337	0.0096	$\{\lambda_2\}$
Murphy's method [32]	0.5410	0.4309	0.0215	0.0065	$\{\lambda_1\}$
Deng et al.'s method [33]	0.7150	0.2546	0.0235	0.0069	$\{\lambda_1\}$
Lin et al's method [6]	0.8749	0.0951	0.0233	0.0066	$\{\lambda_1\}$
Jiang's method [34]	0.8872	0.0832	0.0231	0.0065	$\{\lambda_1\}$
Kaur and Srivastava's method [38]	0.8665	0.1039	0.0231	0.0065	$\{\lambda_1\}$
Proposed method$^{(2)}$	0.8977	0.0691	0.0253	0.0079	$\{\lambda_1\}$
Proposed method$^{(1)}$	0.8976	0.0691	0.0253	0.0080	$\{\lambda_1\}$

(Continued)

Table 8 (continued)

Methods	$\{\lambda_1\}$	$\{\lambda_2\}$	$\{\lambda_2, \lambda_3\}$	Λ	Fault type
Proposed method$^{(1/2)}$	0.8975	0.0691	0.0254	0.0080	$\{\lambda_1\}$
Proposed method$^{(0)}$	0.8973	0.0692	0.0254	0.0081	$\{\lambda_1\}$
Proposed method$^{(-1)}$	0.8965	0.0695	0.0257	0.0082	$\{\lambda_1\}$

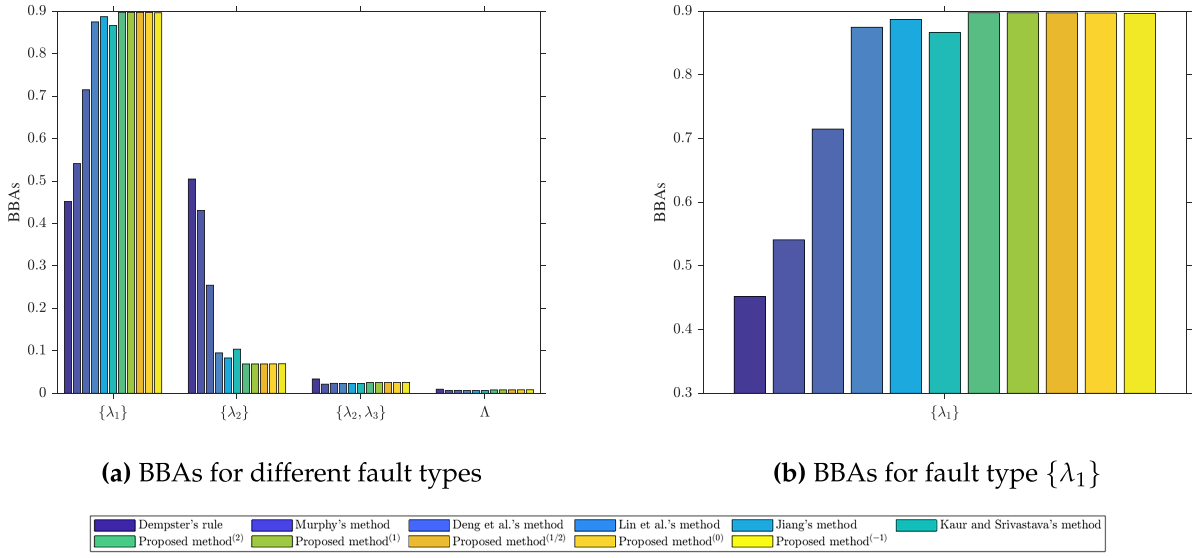

(a) BBAs for different fault types

(b) BBAs for fault type $\{\lambda_1\}$

Figure 7: Results with different methods (a,b) [6,17,32,33,34,38]

5.3 Fault Diagnosis of Automobile System

In this subsection, we implement our proposed method in a case study aimed at diagnosing faults in automobile system. To facilitate this, we employ the dataset from [42], conducting a comparative analysis against other pertinent techniques. In the context of automobile system, operational failures often emerge from prolonged usage, typically originating from one of three principal sources: diminished oil pressure, air leaks in the intake system, and blockages in solenoid valves, denoted as $\{\lambda_1\}$, $\{\lambda_2\}$, and $\{\lambda_3\}$, respectively. To detect and monitor these issues, five sensors are strategically installed within the system to gather pertinent data. This data is then aggregated into BBAs and detailed in Table 9. The frame of discernment is set as $\Lambda = \{\lambda_1, \lambda_2, \lambda_3\}$.

Table 10 presents the outcomes of different methods. A pivotal finding from this table is that despite the initial four sets of evidence primarily indicating fault $\{\lambda_1\}$, the application of Dempster's rule yields surprising outcomes, predominantly influenced by the final piece of evidence which supports $\{\lambda_3\}$. This illustrates a notable shortcoming of Dempster's rule: its inability to handle the fusion of highly conflicting evidence effectively. In comparison, the outcomes of the proposed method are not only able to consistently identify the correct fault type across various sensors but also significantly outperform the alternative methods. This supports the effectiveness of our method in fault diagnosis, especially highlighting its superiority in managing and interpreting data from multiple sources to pinpoint issues within complex systems like automobile system.

Table 9: BBAs in fault diagnosis of automobile system

BBAs	$\{\lambda_1\}$	$\{\lambda_2\}$	$\{\lambda_3\}$	Λ
m_1	0.7	0.1	0	0.2
m_2	0.7	0	0	0.3
m_3	0.65	0.15	0	0.2
m_4	0.75	0	0.05	0.2
m_5	0	0.2	0.8	0

Table 10: Results of different methods

Methods	$\tilde{\mathbf{m}}$	$m_{1,2}$	$m_{1,2,3}$	$m_{1,2,3,4}$	$m_{1,2,3,4,5}$	Fault type
Dempster's rule [17]	$m(\{\lambda_1\})$	0.9032	0.9598	0.9906	0.0000	$\{\lambda_3\}$
	$m(\{\lambda_2\})$	0.0323	0.0249	0.0053	0.3443	
	$m(\{\lambda_3\})$	0.0000	0.0000	0.0008	0.6557	
	$m(\Lambda)$	0.0645	0.0153	0.0033	0.0000	
Murphy's method [32]	$m(\{\lambda_1\})$	0.9032	0.9598	0.9899	0.9715	$\{\lambda_1\}$
	$m(\{\lambda_2\})$	0.0296	0.0241	0.0058	0.0055	
	$m(\{\lambda_3\})$	0.0000	0.0000	0.0008	0.0222	
	$m(\Lambda)$	0.0672	0.0161	0.0035	0.0008	
Deng et al.'s method [33]	$m(\{\lambda_1\})$	0.9032	0.9597	0.9899	0.9933	$\{\lambda_1\}$
	$m(\{\lambda_2\})$	0.0296	0.0243	0.0058	0.0030	
	$m(\{\lambda_3\})$	0.0000	0.0000	0.0008	0.0029	
	$m(\Lambda)$	0.0672	0.0160	0.0035	0.0008	
Lin et al's method [6]	$m(\{\lambda_1\})$	0.9032	0.9597	0.9899	0.9894	$\{\lambda_1\}$
	$m(\{\lambda_2\})$	0.0296	0.0244	0.0058	0.0037	
	$m(\{\lambda_3\})$	0.0000	0.0000	0.0008	0.0061	
	$m(\Lambda)$	0.0672	0.0159	0.0035	0.0008	
Jiang's method [34]	$m(\{\lambda_1\})$	0.9032	0.9598	0.9899	0.9952	$\{\lambda_1\}$
	$m(\{\lambda_2\})$	0.0296	0.0242	0.0058	0.0025	
	$m(\{\lambda_3\})$	0.0000	0.0000	0.0008	0.0015	
	$m(\Lambda)$	0.0672	0.0161	0.0035	0.0008	
Kaur and Srivastava's method [38]	$m(\{\lambda_1\})$	0.9032	0.9597	0.9899	0.9838	$\{\lambda_1\}$
	$m(\{\lambda_2\})$	0.0296	0.0242	0.0058	0.0044	
	$m(\{\lambda_3\})$	0.0000	0.0000	0.0008	0.0110	
	$m(\Lambda)$	0.0672	0.0160	0.0035	0.0008	
Proposed method[(2)]	$m(\{\lambda_1\})$	0.9042	0.9591	0.9894	0.9957	$\{\lambda_1\}$
	$m(\{\lambda_2\})$	0.0256	0.0261	0.0061	0.0026	
	$m(\{\lambda_3\})$	0.0000	0.0000	0.0006	0.0009	
	$m(\Lambda)$	0.0702	0.0148	0.0039	0.0009	

(Continued)

Table 10 (continued)

Methods	$\tilde{\mathbf{m}}$	$m_{1,2}$	$m_{1,2,3}$	$m_{1,2,3,4}$	$m_{1,2,3,4,5}$	Fault type
Proposed method$^{(1)}$	$m(\{\lambda_1\})$	0.9042	0.9590	0.9894	0.9957	$\{\lambda_1\}$
	$m(\{\lambda_2\})$	0.0256	0.0263	0.0061	0.0025	
	$m(\{\lambda_3\})$	0.0000	0.0000	0.0006	0.0009	
	$m(\Lambda)$	0.0702	0.0147	0.0039	0.0009	
Proposed method$^{(1/2)}$	$m(\{\lambda_1\})$	0.9042	0.9590	0.9894	0.9958	$\{\lambda_1\}$
	$m(\{\lambda_2\})$	0.0256	0.0264	0.0062	0.0024	
	$m(\{\lambda_3\})$	0.0000	0.0000	0.0006	0.0009	
	$m(\Lambda)$	0.0702	0.0146	0.0039	0.0009	
Proposed method$^{(0)}$	$m(\{\lambda_1\})$	0.9042	0.9589	0.9894	0.9960	$\{\lambda_1\}$
	$m(\{\lambda_2\})$	0.0256	0.0265	0.0062	0.0022	
	$m(\{\lambda_3\})$	0.0000	0.0000	0.0006	0.0009	
	$m(\Lambda)$	0.0702	0.0145	0.0039	0.0009	
Proposed method$^{(-1)}$	$m(\{\lambda_1\})$	0.9042	0.9603	0.9898	0.9965	$\{\lambda_1\}$
	$m(\{\lambda_2\})$	0.0256	0.0256	0.0059	0.0018	
	$m(\{\lambda_3\})$	0.0000	0.0000	0.0006	0.0009	
	$m(\Lambda)$	0.0702	0.0141	0.0037	0.0008	

Furthermore, we build on a fault diagnosis case study, utilize the scenarios outlined in Table 9. We introduce a variation range of $[-0.1, 0.1]$ that randomly adjusts the confidence value of $\mathbf{m}_1$ across 100 experimental iterations. Following this modification, we apply various fusion methods to analyze the impact of these adjustments on the diagnostic outcomes. This approach allows us to assess the robustness and sensitivity of different fusion techniques under conditions of uncertainty and fluctuation in sensor data. Fig. 8 displays the variation in belief values for the identified fault, as produced by different methods. It is noteworthy that different methods, including Murphy's [32], Deng et al.'s [33], Lin et al.'s [6], Jiang's [34], Kaur and Srivastava's [38], and the proposed method, demonstrate a consistent and strong belief in identifying fault $\{\lambda_1\}$ as the primary issue. Interestingly, our proposed method not only maintains belief values higher than those of the comparative methods but also showcases enhanced diagnostic accuracy and robustness. This highlighting its potential for reliable application in fault diagnosis systems.

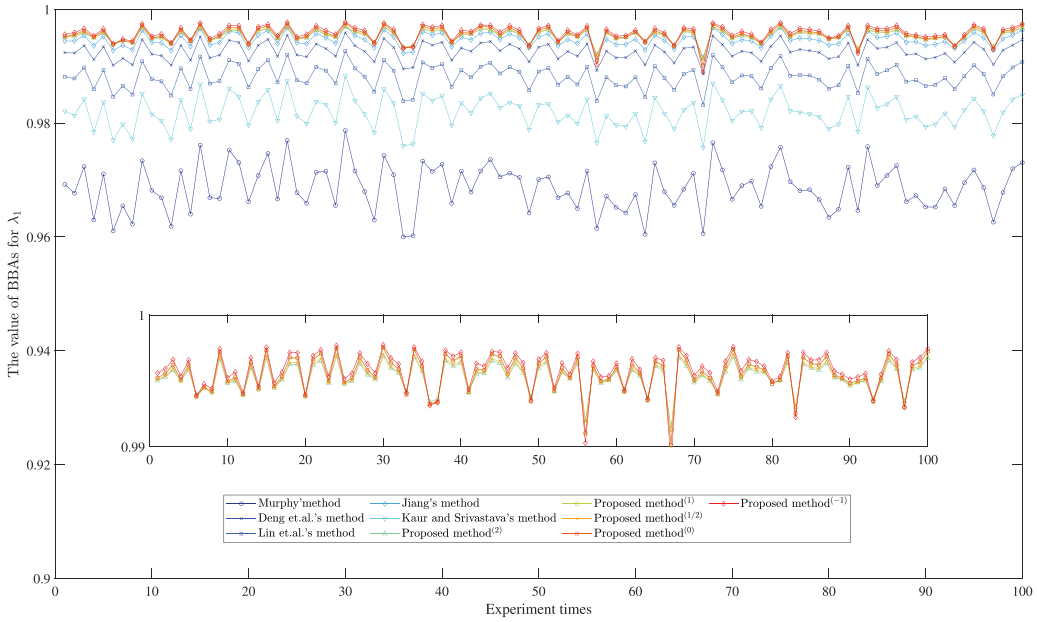

Figure 8: Sensitivity analysis of different methods [6,17,32,33,34,38]

6 Conclusion

In this paper, we introduce a new method, $\mathcal{EJAD}$, based on Dempster-Shafer Theory (DST) specifically designed to address the challenge of resolving highly conflicting evidence. To leverage the inherent discrepancies among subsets and aid in conflict resolution, we further develop an reinforced version, $\mathcal{REJAD}$, which effectively differentiates between subsets containing multiple elements and those with a singleton element. We demonstrate the properties satisfied by the proposed $\mathcal{REJAD}$ and analyze that $\mathcal{REJAD}$ can be related to other divergences, such as χ^2 divergence, Hellinger distance and Jensen-Shannon divergence. The efficacy and rationality of the proposed method are validated through several numerical examples. Building upon this, a new multisensor fault diagnosis method utilizing $\mathcal{REJAD}$ is meticulously crafted. To further substantiate the validity of our method, we apply to three distinct fault diagnosis cases. In comparison to some related methods, our proposed method manifests remarkable superiority, achieving optimal performance in both scenarios. In the future, we aim to explore a wider range of applications for the proposed method, delving into various domains to further establish its versatility and effectiveness in complex data fusion contexts.

Acknowledgement: Not applicable.

Funding Statement: This research received no external funding.

Author Contributions: The authors confirm contribution to the paper as follows: Conceptualization, Zhe Liu; methodology, Zhe Liu; validation, Lili Wang, Yulong Huang and Kai Liu; formal analysis, Juan Liao, Himanshu Dhumras and Wulfran Fendzi Mbasso; investigation, Juan Liao and Yulong Huang; writing—original draft preparation, Zhe Liu, Juan Liao, Lili Wang and Kai Liu; writing—review and editing, Zhe Liu, Yulong Huang, Himanshu Dhumras and Wulfran Fendzi Mbasso; visualization, Lili Wang and Kai Liu; supervision, Zhe Liu. All authors reviewed the results and approved the final version of the manuscript.

Availability of Data and Materials: The data that support the findings of this study are available from the corresponding author, upon reasonable request.

Ethics Approval: Not applicable.

Conflicts of Interest: The authors declare no conflicts of interest to report regarding the present study.

References

1. Ghosh N, Saha S, PaulR. iDCR: improved Dempster combination rule for multisensor fault diagnosis. Eng Appl Artif Intell. 2021;104(4):104369. doi:10.1016/j.engappai.2021.104369.
2. Vashishtha G, Chauhan S, Singh M, Kumar R. Bearing defect identification by swarm decomposition considering permutation entropy measure and opposition-based slime mould algorithm. Measurement. 2021;178:109389. doi:10.1016/j.measurement.2021.109389.
3. Vashishtha G, Chauhan S, Kumar S, Kumar R, Zimroz R, Kumar A. Intelligent fault diagnosis of worm gearbox based on adaptive CNN using amended gorilla troop optimization with quantum gate mutation strategy. Knowl Based Syst. 2023;280:110984. doi:10.1016/j.knosys.2023.110984.
4. Liu Z. An effective conflict management method based on belief similarity measure and entropy for multi-sensor data fusion. Artif Intell Rev. 2023;56(12):15495–522. doi:10.1007/s10462-023-10533-0.
5. Huang H, Liu Z, Han X, Yang X, Liu L. A belief logarithmic similarity measure based on Dempster-Shafer theory and its application in multi-source data fusion. J Intell Fuzzy Syst. 2023;45(3):4935–47. doi:10.3233/jifs-230207.
6. Lin Y, Li Y, Yin X, Dou Z. Multisensor fault diagnosis modeling based on the evidence theory. IEEE Trans Reliab. 2018;67(2):513–21. doi:10.1109/tr.2018.2800014.
7. Wang K, Wang W, Zhao Y, Yuan B, Xiang Z. Multisensor fault diagnosis via Markov chain and evidence theory. Eng Appli Artif Intell. 2023;126(1):106851. doi:10.1016/j.engappai.2023.106851.
8. Zhang H, Deng Y. Weighted belief function of sensor data fusion in engine fault diagnosis. Soft Comput. 2020;24(3):2329–39. doi:10.1007/s00500-019-04063-7.
9. Liu Z, Letchmunan S. Representing uncertainty and imprecision in machine learning: a survey on belief functions. J King Saud Univ Comput Inf. 2024;36(1):101904. doi:10.1016/j.jksuci.2023.101904.
10. Pakhira R, Mondal B, Thirthar AA, Alqudah MA, Abdeljawad T. Developing a fuzzy logic-based carbon emission cost-incorporated inventory model with memory effects. Ain Shams Eng J. 2024;15(6):102746. doi:10.1016/j.asej.2024.102746.
11. Fahmi A, Khan A, Abdeljawad T. Group decision making based on cubic fermatean Einstein fuzzy weighted geometric operator. Ain Shams Eng J. 2024;15(4):102737. doi:10.1016/j.asej.2024.102737.
12. Liu Z. Fermatean fuzzy similarity measures based on tanimoto and sørensen coefficients with applications to pattern classification, medical diagnosis and clustering analysis. Eng Appl Artif Intell. 2024;132(1):107878. doi:10.1016/j.engappai.2024.107878.
13. Xiao F, Wen J, Pedrycz W, Aritsugi M. Complex evidence theory for multisource data fusion. Chin J Inf Fusion. 2024;1(2):134–59. doi:10.62762/cjif.2024.999646.
14. Pan L, Deng Y. A new complex evidence theory. Inf Sci. 2022;608:251–61.
15. Sardar MR, Chakraborty MK. Rough set models of some abstract algebras close to pre-rough algebra. Inf Sci. 2023;621(3–4):104–18. doi:10.1016/j.ins.2022.11.095.
16. Kang Y, Dai J. Attribute reduction in inconsistent grey decision systems based on variable precision grey multigranulation rough set model. Appl Soft Comput. 2023;133(5):109928. doi:10.1016/j.asoc.2022.109928.
17. Dempster A. Upper and lower probabilities induced by a multivalued mapping. Ann Math Stat. 1967;38(2):325–39. doi:10.1214/aoms/1177698950.

18. Shafer G. A mathematical theory of evidence. Vol. 42. Princeton, NJ, USA: Princeton University Press; 1976.
19. Zhu C, Xiao F. A belief Hellinger distance for D-S evidence theory and its application in pattern recognition. Eng Appl Artif Intell. 2021;106(4):104452. doi:10.1016/j.engappai.2021.104452.
20. Liu Z, Letchmunan S. Enhanced fuzzy clustering for incomplete instance with evidence combination. ACM Trans Knowl Discov Data. 2024;18(3):1–20. doi:10.1145/3638061.
21. Luo H, Yang S, Hu X, Hu XX. Agent oriented intelligent fault diagnosis system using evidence theory. Expert Syst Appl. 2012;39(3):2524–31. doi:10.1016/j.eswa.2011.08.104.
22. Yuan K, Deng Y. Conflict evidence management in fault diagnosis. Int J Mach Learn Cybern. 2019;10(1):121–30. doi:10.1007/s13042-017-0704-6.
23. Lu J, Zhang H, Tang X. A novel method for intelligent single fault detection of bearings using SAE and improved D-S evidence theory. Entropy. 2019;21(7):687. doi:10.3390/e21070687.
24. Lyu S, Liu Z. A belief Sharma-Mittal divergence with its application in multi-sensor information fusion. Comput Appl Math. 2024;43(1):1–31. doi:10.1007/s40314-023-02542-0.
25. Liu Z, Cao Y, Yang X, Liu L. A new uncertainty measure via belief Rényi entropy in Dempster-Shafer theory and its application to decision making. Commun Stat-Theory Methods. 2024;53(19):6852–68. doi:10.1080/03610926.2023.2253342.
26. Zhu C, Xiao F, Cao Z. A generalized Rényi divergence for multi-source information fusion with its application in EEG data analysis. Inf Sci. 2022;605(1):225–43. doi:10.1016/j.ins.2022.05.012.
27. Zhang L, Xiao F. A novel belief χ^2 divergence for multisource information fusion and its application in pattern classification. Int J Intell Syst. 2022;37(10):7968–91. doi:10.1002/int.22912.
28. Yager RR. Generalized Dempster-Shafer structures. IEEE Trans Fuzzy Syst. 2019;27(3):428–35. doi:10.1109/tfuzz.2018.2859899.
29. Dubois D, Prade H. Representation and combination of uncertainty with belief functions and possibility measures. Comput Intell. 1988;4(3):244–64. doi:10.1111/j.1467-8640.1988.tb00279.x.
30. Smets P. The combination of evidence in the transferable belief model. IEEE Trans Pattern Anal Mach Intell. 1990;12(5):447–58. doi:10.1109/34.55104.
31. Yager RR. On the Dempster-Shafer framework and new combination rules. Inf Sci. 1987;41(2):93–137. doi:10.1016/0020-0255(87)90007-7.
32. Murphy CK. Combining belief functions when evidence conflicts. Decis Support Syst. 2000;29(1):1–9. doi:10.1016/s0167-9236(99)00084-6.
33. Deng Y, Shi W, Zhu Z, Liu Q. Combining belief functions based on distance of evidence. Decis Support Syst. 2004;38(3):489–93. doi:10.1016/j.dss.2004.04.015.
34. Jiang W. A correlation coefficient for belief functions. Int J Approx Reason. 2018;103:94–106.
35. Xiao F. Multi-sensor data fusion based on the belief divergence measure of evidences and the belief entropy. Inf Fusion. 2019;46(3):23–32. doi:10.1016/j.inffus.2018.04.003.
36. Zhao K, Sun R, Li L, Hou M, Yuan G, Sun R. An improved evidence fusion algorithm in multi-sensor systems. Appl Intell. 2021;51(1):7614–24. doi:10.1007/s10489-021-02279-5.
37. Zhao K, Sun R, Li L, Hou M, Yuan G, Sun R. An optimal evidential data fusion algorithm based on the new divergence measure of basic probability assignment. Soft Comput. 2021;25(17):11449–57. doi:10.1007/s00500-021-06040-5.
38. Kaur M, Srivastava A. A new divergence measure for belief functions and its applications. Int J Gen Syst. 2023;52(4):455–72. doi:10.1080/03081079.2022.2151006.
39. Xiao F, Wen J, Pedrycz W. Generalized divergence-based decision making method with an application to pattern classification. IEEE Trans Knowl Data Eng. 2023;35(7):6941–56. doi:10.1109/tkde.2022.3177896.

40. Chernoff H. A measure of asymptotic efficiency for tests of a hypothesis based on the sum of observations. Ann Math Stat. 1952;23(4):493–507. doi:10.1214/aoms/1177729330.
41. Deng Y. Deng entropy. Chaos Solitons Fractals. 2016;91:549–53.
42. Gao X, Xiao F. A generalized χ^2 divergence for multisource information fusion and its application in fault diagnosis. Int J Intell Syst. 2022;37(1):5–29. doi:10.1002/int.22615.